Modeling of Particulate Matter Creation and Evolution
in Aircraft Engines, Plumes and Particle Sampling Systems

by

Pierre Max Dakhel

Diplomé de l'Ecole Polytechnique (2005)

Ecole Polytechnique, Palaiseau, France

Submitted to the Departement of Aeronautics and Astronautics
in Partial Fulfillment of the Requirements for the Degree of
Master of Science in Aeronautics and Astronautics.

at the Massachusetts Institute of Technology

May 2005 [June 2005]

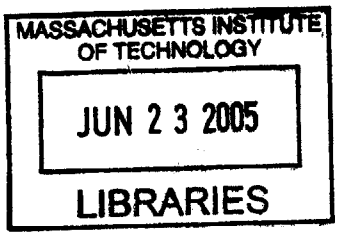

Signature of Author ....

Department of Aeronautics and Astronautics
May 20, 2005

Certified by .....

Ian Waitz
Professor and Deputy Head Department of Aeronautics and Astronautics
Thesis supervisor

Accepted by .....

Jaime Peraire
Professor of Aeronautics and Astronautics
Chair, Committee on Graduate Students

Contents

Abstract

Environmental and health concerns have recently led to growing efforts to characterize the exhaust gas composition of aircraft engines. Besides major chemical species (N_2, O_2, CO_2 and H_2O), aircraft engines also emit other species in much lower concentrations but that may also have significant impacts. Particulate Matter (PM) belongs to this category. This thesis presents a model of the microphysical processes leading to the creation of PM and its subsequent interactions with gas phase chemical species in thermodynamic environments typical of aircraft engines and exhaust plumes at ground level. The effects of the turbine and nozzle of an engine on non-volatile PM emissions are addressed first. Results suggest that limited opportunities exist for the modification of the microphysical properties of the non-volatile PM in these environments, leading to the conclusion that the characteristics of the turbine and nozzle of an aircraft engine have little or no influence on aircraft non-volatile emissions. The analysis is then extended downstream to the case of a plume at ground level. Direct comparisions are made to volatile PM measurements obtained from a recent test (APEX). Time-scale arguments are used to suggest that gas to particle conversion at ground level temperatures is a process too slow for volatile particles to exist before the plume reaches the sampling system and thus little if no modification of the PM characteristics should be measured. However, the residence times and temperatures within the sampling system used in APEX are such that significant modification of the PM characteristics within the sampling system is expected. Recommendations to improve the measuring techniques at ground level include lowering the residence time of gas samples inside the sampling system to avoid too large a modification of the flow microphysical characteristics before it reaches the measuring instruments, and careful monitoring of the temperature of the sample throughout the probe and sampling line.

Introduction

Aircraft emissions have recently received a growing experimental and theoretical interest. They can affect the health and welfare of people living in the neighborhood of airports through changes in air quality, and can also influence climate. The description of the chemical state of the engine exhaust is a necessary prerequisite to assessing the extent of these effects. Exhaust characterization must include the full range of aircraft operating conditions, from ground to flight altitude, and consider the evolution of thermodynamic conditions along a path that includes the intra-engine environment as well as the exhaust plume. Understanding how the chemistry and physics of aircraft particulate matter (PM) develop along this path is a necessary step towards alleviating potential impacts. The exhaust gas of an aircraft is not exclusively composed of gaseous phase chemical species, but also contains liquid (volatile), solid (non-volatile) and mixed (partly volatile and partly non volatile) particles. The combination of the exhaust gas and the other phases in suspension composes what is called an *aerosol*. This thesis is aimed at providing modeling tools necessary to make estimates of the thermodynamics and kinetics of the microphysics of the PM in aeronautical applications.

Exhaust chemistry depends on fuel type, the thermodynamic environment within the engine and in the plume (as driven by thermodynamic cycle, component design, and ambient atmospheric conditions), and also the residence time in any one of these environments, stretching from milliseconds in the combustor and the turbine, to minutes in the plume and days in the subsequent atmospheric processing. To facilitate study of this system from the standpoint of emissions characterization, it is convenient to examine the evolution of the aircraft exhaust in three regions, combustor, turbine-nozzle, and plume. Each region corresponds to a particular thermodynamic environment with a characteristic time-scale and hence, emphasizes different aspects of the chemistry. Rates for the microphysical processes that govern the evolution of non-volatile PM can be determined with the knowledge of the temperature and pressure of the surrounding environment and the initial chemical composition of the fluid. The creation of PM and PM precursors starts in the primary zone of the combustor where black carbon spherules are formed

and where the fuel sulfur is oxidized to sulfur IV. After formation in the primary zone of the combustor, black carbon spherules undergo rapid coagulation and surface growth to form soot. Between the primary zone and the engine exit a proportion of the sulfur is further oxidized and reaches an oxidation number of VI . In addition to soot and sulfur VI, the engine also emits unburned hydrocarbons (HCs) and lubricating oil. Further processing in the plume include conversion of the sulfur VI to sulfuric acid, heterogeneous condensation of exhaust gases and water vapor on emitted non-volatile particles, and the homogeneous nucleation of sulfuric acid droplets.

The description of the physics of aerosols requires statistical tools. They will be introduced in chapter 1 of this document. In chapters 2 to 4, we theoretically describe the process of coagulation which is a key phenomenon for the evolution of the aerosol population and in chapter 5 we will evaluate its effect on the primary emissions. In chapters 5 and 6, we theoretically describe the process of nucleation which takes places in aircraft plumes and in chapter 7 we evaluate its effect in jet exhausts at ground level conditions.

Chapter 1

Statistical Mechanics Basics

Much of the microphysics of particulate matter is driven in some way by collisions (of either particles between themselves or of particles with vapor molecules). It is thus important to be able to compute physical parameters such as speeds, mean free paths and diffusion constants which permit the estimation of collision rates. This is the purpose of this chapter.

We will first review some basic results of statistical mechanics and theory of gases.

1.1 Probability of a state of energy E

Consider a fixed volume containing a fixed amount of particles and in thermodynamic equilibrium. Statistical mechanics proves that the probability for a particle to be in a state characterized by an energy between E and $E + dE$ is proportional to $e^{-\frac{E}{kT}}$ (k Boltzmann constant; T Temperature). In particular, the probability p that a particle has a speed between (v_x, v_y, v_z) and $(v_x + dv_x, v_y + dv_y, v_z + dv_z)$ (characterized by its energy $E = m\dfrac{(v_x^2 + v_y^2 + v_z^2)}{2}$ (m mass of the particle)) is:

$$p \propto e^{-m\left(\frac{v_x^2+v_y^2+v_z^2}{2kT}\right)} dv_x dv_y dv_z \qquad 1.1.1$$

To be an equality, this relation still needs the normalization constant (so as to make the sum of the probabilities equal to one) also called the partition function Z.

$$Z = \int_{-\infty}^{+\infty}\int_{-\infty}^{+\infty}\int_{-\infty}^{+\infty} e^{-m\frac{v_x^2+v_y^2+v_z^2}{2kT}} dv_x dv_y dv_z \quad 1.1.2$$

$$\iff Z = \left(\int_{-\infty}^{+\infty} e^{\left(\frac{mv_x^2}{2kT}\right)} dv_x\right)^3 \quad 1.1.3$$

$$\iff Z = \left(\frac{2kT\pi}{m}\right)^{\frac{3}{2}} \quad 1.1.4$$

So,

$$p = \left(\frac{m}{2kT\pi}\right)^{\frac{3}{2}} e^{-m\left(\frac{v_x^2+v_y^2+v_z^2}{2kT}\right)} dv_x dv_y dv_z \quad 1.1.5$$

1.2 Mean speed, mean square speed

This enables us to calculate two important characteristics of the particle, the mean speed $c = \overline{v}$ and the mean square speed $\overline{v^2}$

1.2.1 Mean speed

$$c * Z = \int_{-\infty}^{+\infty}\int_{-\infty}^{+\infty}\int_{-\infty}^{+\infty} \sqrt{v_x^2+v_y^2+v_z^2}\, e^{-m\left(\frac{v_x^2+v_y^2+v_z^2}{2kT}\right)} dv_x dv_y dv_z \quad 1.2.1$$

We have to make a change of coordinates to be able to compute this by hand. Introducing the momentum $p = m\sqrt{v_x^2+v_y^2+v_z^2}$ we can make a spherical change of coordinates and write $(v_x, v_y, v_z) = \frac{p}{m}(sin\theta cos\phi, sin\theta sin\phi, cos\theta)$ $(0 \leq \theta \leq \pi\ ;\ 0 \leq \phi \leq 2\pi)$. The jacobian of the transformation is $\frac{D(v_x,v_y,v_z)}{D(p,\theta,\phi)} = \frac{1}{m}\left(\frac{p}{m}\right)^2 sin\theta$

$$c * Z = \int_{p=0}^{+\infty} \int_{\theta=0}^{\pi} \int_{\phi=0}^{2\pi} \frac{p}{m} e^{-\left(\frac{p^2}{2mkT}\right)} \frac{1}{m} \left(\frac{p}{m}\right)^2 sin\theta d\theta d\phi dp \quad 1.2.2$$

$$\iff c * Z = \int_{p=0}^{+\infty} e^{-\left(\frac{p^2}{2mkT}\right)} \left(\frac{p}{m}\right)^3 \frac{4\pi}{m} dp \quad 1.2.3$$

$$\iff c * Z = \int_{p=0}^{+\infty} \frac{2p}{m^4} * 4\pi \frac{2kTm}{2} e^{-\left(\frac{p^2}{2kTm}\right)} dp \quad 1.2.4$$

$$\left(\text{by part with } u = \frac{p^2}{m^4} \text{ and } v' = 4\pi p * e^{-\left(\frac{p^2}{2mkT}\right)}\right) \quad 1.2.5$$

$$\iff c * Z = \frac{8\pi kT}{m^3} * \frac{2kTm}{2} \quad 1.2.6$$

$$\iff c = \frac{8\pi(kT)^2}{m^2} * \left(\frac{m}{2kT\pi}\right)^{\frac{3}{2}} \quad 1.2.7$$

$$\iff \quad 1.2.8$$

$$\boxed{c = \left(\frac{8kT}{\pi m}\right)^{\frac{1}{2}}} \quad (1.2.9)$$

1.2.2 Mean square speed

$$\overline{v^2} * Z = \int_{-\infty}^{+\infty} \int_{-\infty}^{+\infty} \int_{-\infty}^{+\infty} \left(v_x^2 + v_y^2 + v_z^2\right) e^{-m\left(\frac{v_x^2+v_y^2+v_z^2}{2kT}\right)} dv_x dv_y dv_z \quad 1.2.10$$

The same change of variables as in the previous section gives:

$$\overline{v^2} * Z = \int_{p=0}^{+\infty} e^{-\left(\frac{p^2}{2mkT}\right)} \left(\frac{p}{m}\right)^4 \frac{4\pi}{m} dp \tag{1.2.11}$$

$$\iff \overline{v^2} * Z = \int_{p=0}^{+\infty} \frac{3p^2}{m^5} \frac{2kTm}{2} e^{-\left(\frac{p^2}{2mkT}\right)} 4\pi dp \tag{1.2.12}$$

$$\iff \overline{v^2} * Z = \int_{p=0}^{+\infty} \frac{3kT}{m^4} \frac{2kTm}{2} e^{-\left(\frac{p^2}{2mkT}\right)} 4\pi dp \tag{1.2.13}$$

$$\iff \overline{v^2} * Z = \frac{3(kT)^2}{m^3} \sqrt{\frac{kTm\pi}{2}} * 4\pi \tag{1.2.14}$$

$$\iff \overline{v^2} = \frac{3(kT)^2}{m^3} \sqrt{\frac{kTm\pi}{2}} * 4\pi * \left(\frac{m}{2kT\pi}\right)^{\frac{3}{2}} \tag{1.2.15}$$

$$\iff \tag{1.2.16}$$

$$\boxed{\overline{v^2} = \frac{3kT}{m}} \tag{1.2.17}$$

(Which when applied to a pure monoatomic gas is nothing else than the famous $U = \frac{3}{2}NkT$ formula)

1.2.3 Remarks

• These results are only true for a particle whose energy is completely concentrated in translation energy (no energy for spinning, no energy for oscillating). However, the effect of those other degrees of liberties or negligeable for aerosol particles in aeronautical applications.

• The results of this part are true for the molecules of a gas as well for the aerosols carried by this gas

1.2.4 Change of frame of reference

Speed

In the next parts of this document, we will often have to consider the mean speed of the particles in the frame of reference of one fixed particle.

Calling u_0 the speed of the particle of reference, the mean kinetic energy of another particle in this frame of reference is:

$$\frac{1}{2}m\overline{(\underline{u}-\underline{u_0})^2} = \frac{1}{2}m\left(\overline{\underline{u^2}}+\overline{\underline{u_0^2}}-2\overline{\underline{u_0}.\underline{u}}\right) \quad 1.2.18$$

$$\iff \frac{1}{2}m\overline{(\underline{u}-\underline{u_0})^2} = \frac{1}{2}m\left(\overline{\underline{u^2}}+\overline{\underline{u_0^2}}\right) \quad 1.2.19$$

$$\iff \frac{1}{2}m\overline{(\underline{u}-\underline{u_0})^2} = m\overline{\underline{u^2}} \quad 1.2.20$$

$$1.2.21$$

Where the assumption that the two movements are independent has been made.

The relative mean square speed has been multiplied by two. The relative speed distribution still having a Gaussian distribution then gives the final argument for saying that the relative mean speed c' is:

$$\boxed{c' = \sqrt{2}c} \quad (1.2.22)$$

Mean free path

With the mean speed being multiplied by $\sqrt{2}$; and the time between two collisions being unchanged, we can conclude that the mean free path (λ_b) of one particle in the frame of reference of another particle is $\sqrt{2}$ times the one in the frame of reference of the observer.

$$\boxed{\lambda_b' = \sqrt{2}\lambda_b} \quad (1.2.23)$$

1.2.5 Change of reference with two different types of particles

Speed

When the change of reference is made for two different types of particles, the above derivation has to be adapted to obtain the relative speed of a particle of type 1 in the frame of reference of a particle of type 2.

$$\frac{1}{2}m_2\overline{(\underline{u_2}-\underline{u_1})^2} = \frac{1}{2}m_2\left(\overline{\underline{u_2}^2}+\overline{\underline{u_1}^2}-2\overline{\underline{u_2}.\underline{u_1}}\right) \quad 1.2.24$$

$$\iff \overline{(\underline{u_2}-\underline{u_1})^2} = \left(\overline{\underline{u_2}^2}+\overline{\underline{u_1}^2}\right) \quad 1.2.25$$

$$\iff \overline{(\underline{u_2}-\underline{u_1})^2} = \left(\frac{3kT}{m_2}+\frac{3kT}{m_1}\right) \quad 1.2.26$$

$$\iff \overline{(\underline{u_2}-\underline{u_1})^2} = 3kT\left(\frac{1}{m_2}+\frac{1}{m_1}\right) \quad 1.2.27$$

$$1.2.28$$

Let's define $\frac{1}{m_{12}} = \frac{1}{m_2} + \frac{1}{m_1}$. The mean square speed changing like this implies that the mean speed becomes:

$$\boxed{c'_2 = \left(\frac{8kT}{\pi m_{12}}\right)^{\frac{1}{2}} = \sqrt{c_1^2+c_2^2}} \quad (1.2.29)$$

Mean free path

The mean free path becomes:

$$\boxed{\lambda'_{b21} = \sqrt{1+\frac{c_1^2}{c_2^2}}\lambda_b} \quad (1.2.30)$$

1.2.6 Collisions

We want the number of collisions that a particle of type 1 (with radius R_{p1}) experiences with particles of type 2 (with radius R_{p2}) per unit time.

A particle of type 2 collides a particle of type 1 if its center is at a distance lower than $R_{p1} + R_{p2}$ from the center of the particle of type 1.

Per unit time, the particle of type 1 collides with the particles of type 2 whose centers are within a volume $\pi\left(R_{p1}+R_{p2}\right)^2 * c$. In this volume there are $\pi\left(R_{p1}+R_{p2}\right)^2 * cN_2$ particles of type 2 (N_2 is the concentration of particles of type 2)

The speed c here is the mean relative speed of a particle of type 1 in the frame of reference of a particle of type 2 ($c = \sqrt{c_1^2+c_2^2}$). Finally the number of collisions is:

$$\boxed{Z = \pi\sqrt{c_1^2 + c_2^2}\left(R_{p1} + R_{p2}\right)^2 N_2} \tag{1.2.31}$$

Which still has to be multiplied by N_1 (the concentration of particles of type 1) to have the total number of collisions per unit time per unit volume occurring between the two aerosols 1 and 2

1.3 Diffusion

1.3.1 Flux of particles through a surface

We are interested in the number of particles which are crossing a plane in one direction.

To simplify, we consider that all particles have the same speed c. During a short time t (typically a time shorter than the one required for a particle to collide with another particle), the particles move in straight lines and cover a distance $L = c * t$

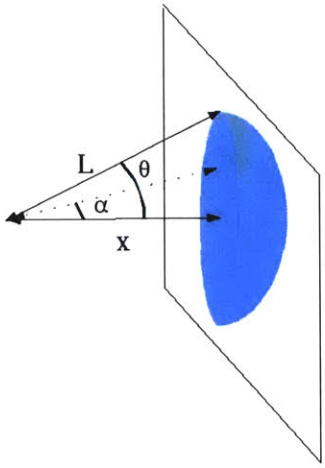

Figure 1.1:

Only particles at a distance x smaller than L have a chance to cross the plane. Those who could cross are those whose speeds are within a precise solid angle Ω.

$$\Omega = \frac{S}{L^2} \text{ with } \quad S = \int_{\alpha=0}^{\theta} 2\pi L sin\alpha L d\alpha \tag{1.3.1}$$

$$\iff \quad S = 2\pi L^2 (1 - cos\theta) \tag{1.3.2}$$

$$\iff \quad S = 2\pi L^2 \left(1 - \frac{x}{L}\right) \tag{1.3.3}$$

$$\iff \quad \Omega = 2\pi \left(1 - \frac{x}{L}\right) \tag{1.3.4}$$

Per unit of surface of the plan, the particles located between x and $x + dx$ contribute $\frac{\Omega N}{4\pi} dx$ (where N is the density of particles) to the total of particles that crossed.
So the number of particles crossing per unit of surface is

$$\int_{x=0}^{L} \frac{\Omega N}{4\pi} dx \quad = N \int_{x=0}^{L} \frac{1}{2} \left(1 - \frac{x}{L}\right) \quad = \frac{NL}{4} \tag{1.3.5}$$

Remembering that $L = ct$, the final interesting result is that per unit of surface and per unit of time the number of particle crossing is:

$$\boxed{J_0 \quad = \quad \frac{Nc}{4}} \tag{1.3.6}$$

Remark

• We supposed that the density N was constant over $[0\ ,\ L]$. When this is not the case, it is often replaced by its mean value at $x = \lambda_b$ where λ_b is the mean free path.

1.3.2 Net flux of particles through a surface

The previous result gives us the flux in one direction. However, if the concentration of the particles on the other side is not zero, this flux is going to be compensated by the arrival of particles from the other side.

If we arbitrarily say that all particles crossing the plane during the time t were at a distance λ from the wall (which is not correct, but let's consider that it was a mean distance from the wall)

The net flux is:

$$J = J_0(x-\lambda) - J_0(x+\lambda) \quad (1.3.7)$$

$$J = \frac{N(x-\lambda)c}{4} - \frac{N(x+\lambda)c}{4} \quad (1.3.8)$$

$$J = -\frac{\lambda c}{2} * \frac{dN}{dx} \quad (1.3.9)$$

$$\boxed{J = -D * \frac{dN}{dx}} \quad (1.3.10)$$

Remarks

• This formula is only valid when we consider the transport of particles over distance larger than a mean free path. If this is not the case, we can not approximate the differences between the flux in one direction and the one in the other direction with a derivative.

• The distance λ needs some more comments. It is the "mean" distance from the wall at which the particles which could cross the plane during the short time t were located. We said that the time t had to be short enough to make sure that the particles did not have time to collide with each other. Some people then take t as the mean time between two collisions and hence also say that λ is mean free path (let's call it λ_b). However, this is not extremely rigorous. Although the mean free path is a rigorous concept, we cannot rigorously say that $D = \frac{\lambda_b c}{2}$ and effectively people disagree on this. Some authors write $D = \frac{4\lambda_b c}{\sqrt{\pi}}$ others $D = \frac{\pi\lambda_b c}{8}$ and one is able to find a whole series of similar formulas. The practical conclusion of this is that one should later avoid to split the coefficient D in a product of the form $A * \lambda_b c$.

• Two different aerosols have different mean free paths and hence different diffusion constants which are also different from the mean free path of the carrier gas in itself.

1.3.3 Fick's law

The last formula can be easily generalized to any surface. If $\underline{n}dS$ is an elementary oriented surface, the net flux through it in the direction of $\underline{n}$ is:

$$dJ = -D * \underline{grad}(N) \cdot \underline{n}dS \quad (1.3.11)$$

or

$$\boxed{\underline{J} = -D * \underline{grad}(N)} \tag{1.3.12}$$

Writing the conservation of particles in a volume, we have:

$$\frac{\partial N}{\partial t} + div(\underline{J}) = 0 \tag{1.3.13}$$

$$\boxed{\frac{\partial N}{\partial t} = D\nabla^2 N} \tag{1.3.14}$$

We can also remember that the conservation of the number of particles can also be written as:

$$\frac{\partial N}{\partial t} + div(N\underline{u}) = 0 \tag{1.3.15}$$

Which compared to the previous equation gives Fick's law:

$$\boxed{N\underline{u} = -D * \underline{gradN}} \tag{1.3.16}$$

Remark

• The speed $\underline{u}$ in the last definition does not refer to the global speed of the medium, but to the speed of the species which we write the formula for.

1.3.4 Important application

Consider N_0 aerosol particles and a carrier gas. Imagine that at t=0, we put all N_0 aerosol particles at the point $(x, y, z) = (0, 0, 0)$. The formula $\frac{\partial N}{\partial t} = D\nabla^2 N$ enables to track the evolution of the aerosols and to find some characteristics of the distribution. Multiplying it by $r^2 = x^2 + y^2 + z^2$ and integrating over the whole space, we obtain:

$$\int_{x=-\infty}^{+\infty}\int_{y=-\infty}^{+\infty}\int_{z=-\infty}^{+\infty} r^2 \frac{\partial N}{\partial t} dxdydz = \int_{x=-\infty}^{+\infty}\int_{y=-\infty}^{+\infty}\int_{z=-\infty}^{+\infty} (x^2+y^2+z^2) D\left(\frac{\partial^2 N}{\partial x^2} + \frac{\partial^2 N}{\partial y^2} + \frac{\partial^2 N}{\partial z^2}\right) dxdydz$$

but: $$\int_{x=-\infty}^{+\infty}\int_{y=-\infty}^{+\infty}\int_{z=-\infty}^{+\infty} x^2\frac{\partial^2 N}{\partial y^2}dxdydz = \int_{x=-\infty}^{+\infty}\int_{z=-\infty}^{+\infty} x^2 * \underbrace{\left[\frac{\partial N}{\partial y}\right]_{-\infty}^{+\infty}}_{=0} dxdz = 0$$

and:

$$\int_{x=-\infty}^{+\infty}\int_{y=-\infty}^{+\infty}\int_{z=-\infty}^{+\infty} r^2\frac{\partial N}{\partial t}dxdydz = \frac{\partial}{\partial t}\int_{x=-\infty}^{+\infty}\int_{y=-\infty}^{+\infty}\int_{z=-\infty}^{+\infty} r^2 N = N_0\frac{\partial \overline{r^2}}{\partial t}$$

So we have:

$$N_0\frac{\partial \overline{r^2}}{\partial t} = \int_{x=-\infty}^{+\infty}\int_{y=-\infty}^{+\infty}\int_{z=-\infty}^{+\infty}(x^2 D\frac{\partial^2 N}{\partial x^2} + y^2 D\frac{\partial^2 N}{\partial y^2} + z^2 D\frac{\partial^2 N}{\partial z^2})dxdydz \quad 1.3.18$$

Integrating the right hand side twice by part gives:

$$N_0\frac{\partial \overline{r^2}}{\partial t} = 6DN_0 \quad 1.3.19$$

$$\boxed{\overline{r^2} = 6Dt} \quad (1.3.20)$$

and also

$$\overline{x^2} = \overline{y^2} = \overline{z^2} = 2Dt \quad 1.3.21$$

• This formula describes the spread of N_0 particles concentrated at $t = 0$ in one point of the carrier gas. It gives the mean distance made by one particle after a time t. (In the carrier gas frame of reference)

1.3.5 Computation of the diffusion constant with Stoke's law

The statistical description of particles composing the aerosol can be enhanced by the introduction of Stoke's law. Stoke's law says that at low Reynolds number, a rigid spherical particle of radius R_p and speed $\underline{u}$ sees the carrier fluid apply a force on it whose expression is:

$$\underline{F} = -6\pi\mu R_p\underline{u} \quad 1.3.22$$

However, this formula supposes a continuous medium which will not necessarily be the case at the very small scales commom is aerosol mechanics. The formula is then corrected to:

$$\underline{F} = -\frac{6\pi\mu R_p \underline{u}}{C_c} \tag{1.3.23}$$

where C_c is a empirical function of the ratio $\frac{R_p}{\lambda_b}$ (λ_b is the mean free path of the particle in the carrier medium).

$$C_c = 1 + \frac{\lambda}{R_p}\left[1.257 + 0.4e^{-\frac{1.1*R_p}{\lambda}}\right] \tag{1.3.24}$$

Equation of motion

If the only force applied on the particle were the Stoke's force, the particle would come to rest. However, we demonstrated in a previous section that the particle's mean square speed ($\sim$ kinetic energy) is a contant: $\overline{v^2} = \frac{3kT}{m}$. That implies that the particle experiences some acceleration $\underline{a}$. This acceleration is due to the collisions with the molecules of the carrier gas.

The equation of motion is:

$$m\frac{d\underline{v}}{dt} = -\frac{6\pi\mu R_p}{C_c}\underline{v} + m\underline{a} \tag{1.3.25}$$

$$\iff \frac{d\underline{v}}{dt} = -\frac{1}{\tau}\underline{v} + \underline{a} \qquad \tau = \frac{mC_c}{6\pi\mu R_p} \tag{1.3.26}$$

$$\implies \overline{\underline{r}.\frac{d\underline{v}}{dt}} = -\frac{1}{\tau}\overline{\underline{r}.\underline{v}} + \overline{\underline{r}.\underline{a}} \qquad \text{multiplication by } \underline{r} \text{ and ensemble averaging} \tag{1.3.27}$$

$$\implies \overline{\underline{r}.\frac{d\underline{v}}{dt}} = -\frac{1}{\tau}\overline{\underline{r}.\underline{v}} \qquad \underline{a} \text{ and } \underline{r} \text{ are independent and } \overline{\underline{a}} = 0 \tag{1.3.28}$$

$$\implies \frac{d}{dt}\overline{\underline{r}.\underline{v}} = -\frac{1}{\tau}\overline{\underline{r}.\underline{v}} + \overline{v^2} \tag{1.3.29}$$

$$\implies \frac{d}{dt}\overline{\underline{r}.\underline{v}} = -\frac{1}{\tau}\overline{\underline{r}.\underline{v}} + \frac{3kT}{m} \tag{1.3.30}$$

$$\implies \overline{\underline{r}.\underline{v}} = \frac{3kT\tau}{m} + ce^{-\frac{t}{\tau}} \tag{1.3.31}$$

$$\implies \frac{1}{2}\frac{d}{dt}\overline{r^2} = \frac{3kT\tau}{m} + ce^{-\frac{t}{\tau}} \tag{1.3.32}$$

$$\implies \frac{d}{dt}\overline{r^2} = \frac{6kT\tau}{m} + ce^{-\frac{t}{\tau}} \tag{1.3.33}$$

If we wait sufficiently long, the statistical fluctuation due to the exponential disappears and we end up with:

$$\boxed{\overline{r^2} = \frac{6kT\tau}{m}t} \tag{1.3.34}$$

which compared to the formula of the last section gives a expression for the diffusion D:

$$\boxed{D = \frac{kTC_c}{6\pi\mu R_p}} \tag{1.3.35}$$

• $\tau = \frac{mC_c}{6\pi\mu R_p}$ is called the relaxation time of the particle. It is interpreted as the characteristic time required for the particle to change its direction. In the case of a "*large*" aerosol, for which defining the mean free path by the mean distance between 2 collisions with a gas molecule is not valid because of the large number of gas molecules hitting it all the time, a "mean free path" can be defined by means of $\lambda_b = c_b\tau$

Mobility

If a macroscopic force $\underline{F}_{ext}$ is superimposed in the equation of motion, it becomes:

$$m\frac{d\underline{v}}{dt} = \underline{F}_{ext} - \frac{m}{\tau}\underline{v} + m\underline{a} \qquad 1.3.36$$

Ensemble averaging gives:

$$0 = \underline{F}_{ext} - \frac{m}{\tau}\overline{\underline{v}} \qquad 1.3.37$$

Which gives the mean speed:

$$\overline{\underline{v}} = \frac{\underline{F}_{ext}\tau}{m} \qquad 1.3.38$$

We see that the mean speed is proportional to the force. The coefficient of proportionality is called the mobility and is noted B ($\overline{\underline{v}} = B\underline{F}_{ext}$). Some elementary calculations give $B = \frac{D}{kT} = \frac{C_c}{6\pi\mu R_p}$

Chapter 2

Brownian Coagulation

The work in this chapter is based on [9]

2.1 Foreword

This foreword aims at introducing an important parameter: the **Knudsen** number. Condensation and coagulation processes can be categorized by forming the nondimensional ratio of the following two quantities:

- The radius a of the absorbing particle
- The mean free path λ of the coagulated (or absorbed or condensed) particle

$$\boxed{Kn = \frac{\lambda}{a}} \tag{2.1.1}$$

We will see that there will be three regimes:

$Kn \ll 1$	Continuous regime
$Kn \gg 1$	Free molecular regime
Otherwise	Intermediate regime

The mean path of a particle being a decreasing function of its radius, we can anticipate that big absorbed particles (like for soot-soot coagulation) will evolve close to the continuous regime whereas small absorbed particles (like H_2SO_4 condensing on soot) will evolve close to the free molecular regime.

In the rest of this section, we fix a sphere of radius a at the origin of a spherical set of coordinates and we consider only an isotropic space ($\frac{\partial}{\partial\theta} = \frac{\partial}{\partial\varphi} = 0$)

2.2 Perfect continuous regime

2.2.1 Fixed absorbing or exsorbing aerosol

Consider a carrier gas at rest (no shear, no acceleration) and aerosols diffusing inside it. Let's imagine that at $t = 0^-$ the aerosol population is uniform and that at $t = 0$ the particles start coagulating.

To simplify, all particles (apart from the sphere of radius a at the origin) will be point particles (the general case will be described later).

$Kn \ll 1$ implies that Fick's law is applicable everywhere in the space: The following statement can be taken as the definition of what we call the continuous regime:

The flux dJ of particles through an elementary surface $\underline{n}dS$ is :

$$\boxed{dJ_c = -D * \underline{grad}(N) \cdot \underline{n}dS} \tag{2.2.1}$$

Where N is the concentration of aerosols. The subscript $_c$ stands for 'continuous'.

Integrating over the surface of the center sphere and considering concentration distributions only function of r (isotropy of space), we have:

$$J_c = 4\pi a^2 D \left(\frac{\partial N}{\partial r}\right)_{r=a} \tag{2.2.2}$$

We need $\frac{\partial N}{\partial r}$. We calculate it using the following law:

$$\frac{\partial N}{\partial t} = D\nabla^2 N \tag{2.2.3}$$

Now, we have to be careful about the boundary conditions. We will look at the two extreme cases:

• If we consider absorption (coagulation) on the center sphere, the boundary conditions will be:

$$N(\infty,t) = N_\infty \ \forall t \quad 2.2.4$$
$$N(a,t) = 0 \ \forall t \quad 2.2.5$$
$$N(r,0) = N_\infty \ r > a \quad 2.2.6$$

Where N_0 is the concentration of aerosol far from the absorbing particle

• If we consider exsorption (evaporation) from the center sphere, the boundary conditions will be:

$$N(\infty,t) = 0 \ \forall t \quad 2.2.7$$
$$N(a,t) = N_s \ \forall t \quad 2.2.8$$
$$N(r,0) = 0 \ r > a \quad 2.2.9$$

Where N_s is the saturation concentration of the aerosol.

The solutions are:

$$N_{co}(r,t) = N_\infty \left[1 - \frac{a}{r} + \frac{2a}{r\sqrt{\pi}} \int_0^{\frac{r-a}{2\sqrt{Dt}}} e^{-\eta^2} d\eta\right] \quad 2.2.10$$

and:

$$N_{ev}(r,t) = N_s \left[\frac{a}{r} - \frac{2a}{r\sqrt{\pi}} \int_0^{\frac{r-a}{2\sqrt{Dt}}} e^{-\eta^2} d\eta\right] \quad 2.2.11$$

What is convenient about these two extreme solutions is that the boundary conditions don't overlap each other so that, the equation being linear, one can create more general solutions by making linear combinations of $N_{co}(r,t)$ and $N_{ev}(r,t)$.

The gradients are:

$$\left(\frac{\partial N_{co}}{\partial r}\right)_{r=a} = N_\infty \left[\frac{1}{a} + \frac{1}{\sqrt{\pi Dt}}\right] \quad 2.2.12$$
$$\left(\frac{\partial N_{ev}}{\partial r}\right)_{r=a} = -N_s \left[\frac{1}{a} + \frac{1}{\sqrt{\pi Dt}}\right] \quad 2.2.13$$

And finally the fluxes are:

$$J_{c_{co}} = 4\pi a D N_0 \left(1 + \frac{a}{\sqrt{\pi D t}}\right) \quad 2.2.14$$

$$J_{c_{ev}} = -4\pi a D N_s \left(1 + \frac{a}{\sqrt{\pi D t}}\right) \quad 2.2.15$$

We can eliminate $\frac{a}{\sqrt{\pi D t}}$ by noting that for most applications $D \sim 10^{-6} - 10^{-9} m^2 s^{-1}$ and $a \leq 10^{-6} m$ so that after $1ms$ $\frac{a}{\sqrt{\pi D t}} \ll 1$.

Finally,

$$J_{c_{co}} = 4\pi a D N_\infty \quad 2.2.16$$

$$J_{c_{ev}} = -4\pi a D N_s \quad 2.2.17$$

For soot-soot interaction, the real flux J will be reduced to J_{co} because no particle will evaporate: $J_c = 4\pi a D N_\infty$.

For condensation of sulfuric acid on soot, the real flux J_c will be the sum of $J_{c_{co}}$ and $J_{c_{ev}}$ because H_2SO_4 molecules do evaporate: $J_c = 4\pi a D(N_\infty - N_s)$

There have been a number of simplifications in this part (aerosol modeled as point particles and a fixed absorbing central sphere) that make this result only approximate. The next section explains what corrections are necessary.

2.2.2 Moving absorbing or exsorbing aerosol

This part aims at correcting the formula obtained in the previous part where the absorbing particle was considered fixed and were the aerosols were point particles.

The central sphere will now be labeled as particle 1 (radius a_1, diffusivity D_1) and the aerosol will be particle 2 (radius a_2, diffusivity D_2).

First, a has to be replaced by $a_1 + a_2$. Indeed, a particle is absorbed if its center is located at a distance $a_1 + a_2$ of the center of the absorbing particle. Hence we can substitute the geometry of a particle of radius a_1 absorbing a particle of radius a_2 by a geometry where the absorbing particle would have a radius $a_1 + a_2$ and the absorbed particle were a point particle.

Another correction has to be done on D which in the previous part was the diffusion constant of the particle in the carrier gas. Now, when we consider the diffusion of aerosol

2 in the frame of reference of aerosol 1, we have to change Fick's law by using the diffusion constant D_{12} of 2 in 1:

$$\frac{\partial N_2}{\partial t} = D_{12}\nabla^2 N_2 \qquad 2.2.18$$

Remembering that this equation directly implies $\overline{x^2} = 2Dt$ we have a means to access D_{12} by calculating the variance of the displacement of a particle of 2 in the frame of reference of a particle of 1.

$$\overline{(x_2 - x_1)^2} = \overline{x_2^2} + \overline{x_1^2} + \overline{x_1 x_2} \qquad 2.2.19$$
$$\iff \overline{(x_2 - x_1)^2} = 2D_1 t + 2D_2 t + 0 \qquad 2.2.20$$
$$\iff D_{12} = D_1 + D_2 \qquad 2.2.21$$

Finally, by doing the same calculations as in the previous part, we find:

$$J_{c_{ab}} = 4\pi(a_1 + a_2)(D_1 + D_2)N_{2\infty} \qquad 2.2.22$$
$$J_{c_{ev}} = -4\pi(a_1 + a_2)(D_1 + D_2)N_{2s} \qquad 2.2.23$$
$$J_c = 4\pi(a_1 + a_2)(D_1 + D_2)(N_{2\infty} - N_{2s}) \qquad 2.2.24$$

These results are per particle of type 1. If we want a result per unit volume:

$$\boxed{J_c = 4\pi(a_1 + a_2)(D_1 + D_2)N_1(N_{2\infty} - N_{2s})} \qquad (2.2.25)$$

When the two particles are of the same type, the above formula has to be divided by two has each collision (or exsorption) would then have been counted twice ($J_{c_{ab}} = 8\pi a D N^2$, $J_{c_{ev}} = -8\pi a D N^2$).

2.3 Free molecular regime

When the Knudsen number is infinite, we are under what is called a purely molecular regime. It can be shown that under such circumstances, the flux through a elementary surface $\underline{dS}$ is equal to $\underline{dJ} = \frac{1}{4}cN\underline{dS}$ (where c is the mean thermal speed of the aerosol and N is the concentration at a distance equal to the mean free path from the elementary surface.

The corresponding fluxes for a fixed central sphere with point particle around it are:

$$J_{f_{ab}} = \pi a^2 \beta c N_\infty \quad (2.3.1)$$
$$J_{f_{ev}} = -\pi a^2 \beta c N_s \quad (2.3.2)$$

Where β is the sticking probability. The subscript $_f$ stands for free molecular.
If we correct those formula as in the previous part we get:

$$J_{f_{ab}} = \pi (a_1 + a_2)^2 \beta \sqrt{c_1^2 + c_2^2} N_{2\infty} \quad (2.3.3)$$
$$J_{f_{ev}} = -\pi (a_1 + a_2)^2 \beta \sqrt{c_1^2 + c_2^2} N_{2s} \quad (2.3.4)$$

2.4 Intermediate regime

In real life, the Knudsen number is neither 0 nor $+\infty$ so that the flux will be somewhere between the continuous regime and the free molecular regime.

2.4.1 Low corrections

One of the major correction ideas is due to Fuchs and consists in introducing a boundary sphere around the absorbing particle. Outside this boundary sphere, the flux of particle is supposed to be driven by a continuous diffusion process, inside the boundary sphere, the flux is supposed to be in the free molecular regime. The two fluxes are set equal at the boundary. Applying this idea for a boundary sphere located at a distance δ from the surface gives:

Outer part $(r \geq a + \delta)$

$$J_c = 4\pi D (a + \delta)(N_\infty - N') \quad (2.4.1)$$

N' is the concentration at the distance δ from the absorbing sphere

Inner part $(a \leq r \leq a + \delta)$

$$J_f = \pi a^2 \beta c (N' - N_s) \quad (2.4.2)$$

Matching

By equating the two fluxes, we can eliminate N' and find the new expression of the flux.

$$N' = \frac{a^2\beta c N_s + 4(a+\delta)DN_\infty}{a^2\beta c + 4(a+\delta)D} \tag{2.4.3}$$

and

$$\boxed{J = \frac{4\pi aD}{\frac{a}{a+\delta}+\frac{4D}{ac\beta}}(N_\infty - N_s)} \tag{2.4.4}$$

To make the Knudsen number appear in this formula, the distance δ is written as $\delta = \alpha\lambda$ and the diffusion as $D = \frac{1}{3}c\lambda$, so that

$$J = \frac{J_c}{\frac{1}{1+\alpha Kn} + \frac{4Kn}{3\beta}} \tag{2.4.5}$$

Where J_c is the flux as if we were in a purely continuous regime. J_c can be the one for condensation or evaporation.

Depending on the nature of the problem, there will be different formulas to get δ.

2.4.2 High corrections

The latest formula matches the measurements well for not too high Knudsen number, however for $Kn \to \infty$, some authors pointed out that stronger corrections are required.

For the case of higher Knudsen number, new correction methods have to be used. The most used one consists of finding the Maxwell distribution of speeds modified by the presence of the absorbing particle and the result is:

$$J = \frac{J_c(Kn+1)}{0.337Kn + 1 + \frac{4}{3}\frac{Kn^2}{\beta} + \frac{4}{3}\frac{Kn}{\beta}} \tag{2.4.6}$$

2.4.3 Fuchs' method to get δ

In Fuchs' definition, δ is the mean distance from the absorbing sphere of the particles at their last collision before being absorbed.

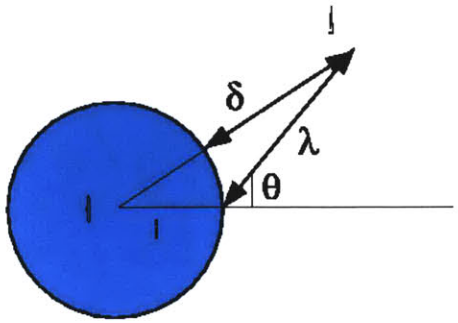

Figure 2.1:

We have:

$$OA^2 = a^2 + \lambda^2 - 2a\lambda cos(\pi - \theta) \quad 2.4.7$$

$$2.4.8$$

The particles arriving between θ and $\theta + d\theta$ are in the elementary solid angle:

$$d\Omega = \frac{2\pi sin\theta\lambda\lambda d\theta}{\lambda^2} = 2\pi sin\theta d\theta \quad 2.4.9$$

So:

$$\overline{OA} = \frac{1}{2\pi}\int_{\theta=0}^{\frac{\pi}{2}} \sqrt{a^2 + \lambda^2 + 2a\lambda cos(\theta)} * 2\pi sin\theta d\theta \quad 2.4.10$$

$$\iff \overline{OA} = \frac{1}{3a\lambda}\left((a+\lambda)^3 - (a^2+\lambda^2)^{\frac{3}{2}}\right) \quad 2.4.11$$

$$\iff \delta = \frac{1}{3a\lambda}\left((a+\lambda)^3 - (a^2+\lambda^2)^{\frac{3}{2}}\right) - a \quad 2.4.12$$

$$2.4.13$$

Now, as usual we will need to make corrections to get the formula for the case when the absorbing sphere is moving and when the aerosol is not composed of point particles. Fuchs simplifies those corrections are simply writes: $\delta = \sqrt{\delta_1^2 + \delta_2^2}$. This formula is only approximate but practical.

Final formula with Fuch's correction

With all the corrections, the final flux per unit volume becomes:

$$\boxed{J_{12} = \frac{4\pi(a_1+a_2)(D_1+D_2)}{\frac{(a_1+a_2)}{(a_1+a_2)+\sqrt{\delta_1^2+\delta_2^2}}+\frac{4(D_1+D_2)}{\beta\sqrt{c_1^2+c_2^2}(a_1+a_2)}} N_1(N_{2\infty} - N_{2s})} \tag{2.4.14}$$

Chapter 3

Electrically enhanced coagulation

The work in this chapter is based on [13].

3.1 Correction in the continuous regime

We now analyze the case in the continuous regime when there is a force $\underline{F}$ deriving from a potential ψ between the particles.

Fick's law:

$$\underline{J} = -D * \underline{grad}(N) \tag{3.1.1}$$

But this formula supposes that there is no macroscopic movement of particles superimposed on the system by a velocity field. If such a velocity field $\underline{V}$ exists, the latter formula is changed to:

$$\underline{J} = -D * \underline{grad}(N) + N\underline{V} \tag{3.1.2}$$

Which, when used with the mass conservation law $\frac{\partial N}{\partial t} + div(\underline{J}) = 0$ yields:

$$\frac{\partial N}{\partial t} = D\nabla^2 N - div(N\underline{V}) \tag{3.1.3}$$

In our case, $\underline{V} = B\underline{F}$ so that:

$$\frac{\partial N}{\partial t} = D\nabla^2 N - Bdiv(N\underline{F}) \tag{3.1.4}$$

We will now consider a steady state ($\frac{\partial N}{\partial t} = 0$) and rewrite the equation in spherical coordinates. Placing the center of the system of coordinates at the center of the particle and using the spherical symmetry, we get:

$$0 = D\frac{1}{r^2}\frac{\partial}{\partial r}\left(r^2\frac{\partial N}{\partial r}\right) - B\frac{1}{r^2}\frac{\partial}{\partial r}\left(r^2 N F_r\right) \tag{3.1.5}$$

$$\iff cst = 4\pi r^2\left(D\frac{\partial N}{\partial r} - BNF_r\right) \tag{3.1.6}$$

Where we can identify the constant with J_c, the flux through a sphere concentric to the particle.

$$J_c = 4\pi r^2\left(D\frac{\partial N}{\partial r} - BNF_r\right) \tag{3.1.7}$$

We now need to find the function $N(r)$ to find this flux. By changing the unknown to $q = Ne^{-\frac{B}{D}\int_r^\infty F}$ we have:

$$\frac{\partial q}{\partial r} = \frac{J_c e^{-\frac{B}{D}\int_r^\infty F}}{4\pi D r^2} \tag{3.1.8}$$

when integrated with the boundary conditions $N(a) = N_s$ and $N(\infty) = N_\infty$ and by using that $\frac{B}{D} = \frac{1}{kT}$ and denoting the potential $\psi(r) = -\int_r^\infty F(r)dr$ it yields:

$$\boxed{J_c = \frac{4\pi D(N_\infty - N_s e^{\frac{\psi(a)}{kT}})}{\int_a^\infty \frac{1}{r^2} e^{\frac{\psi(r)}{kT}}}} \tag{3.1.9}$$

Finally, the usual corrections give:

$$\boxed{J_c = \frac{4\pi(D_1+D_2)(N_{2\infty} - N_{2s} e^{\frac{\psi(a)}{kT}})}{\int_{a_1+a_2}^\infty \frac{1}{r^2} e^{\frac{\psi(r)}{kT}}} N_1} \tag{3.1.10}$$

3.1.1 Case of pure Coulombic interaction

In the case of a Coulomb interaction with no evaporation:

$$\int_a^\infty \frac{1}{r^2} e^{\frac{q_1 q_2}{4\pi\epsilon_0 kTr}} dr \quad = \int_0^{\frac{1}{a}} e^{\frac{q_1 q_2 s}{4\pi\epsilon_0 kT}} ds \quad = 4\pi\epsilon_0 kT \frac{e^{\frac{q_1 q_2}{4\pi\epsilon_0 akT}} - 1}{q_1 q_2} \tag{3.1.11}$$

$$\boxed{J_c \quad = 4\pi(D_1 + D_2) \left[\frac{\frac{q_1 q_2}{4\pi\epsilon_0 kT}}{\left(e^{\frac{q_1 q_2}{4\pi\epsilon_0 (a_1 + a_2) kT}} - 1 \right)} \right] N_1 N_2} \tag{3.1.12}$$

3.2 Correction in the free molecular regime

3.2.1 Impact parameter

We will compute here the enhancement factor $E.F$ of coagulation when there is an attractive force deriving from a central potential U between the absorbing particles and the absorbed particles.

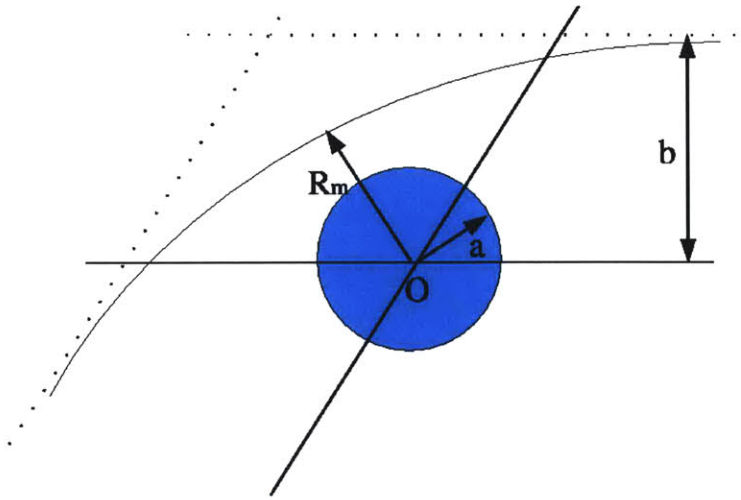

Figure 3.1: Increase of impact diameter

In the absence of forces and in the free molecular regime, the number of particles hitting the blue absorbing sphere is:

$$J_f = \pi a^2 N c \tag{3.2.1}$$

where N is the concentration of absorbed particles (at a distance equal to the mean free path from the absorbing particle)

Now, if we add an attractive (potential) force, we see that the particles approach the absorbing sphere to the distance R_m which is shorter than the distance b (called impact parameter) which represents the minimum distance that there would have been between the sphere and the trajectory of the particle in the absence of forces.

If $R_m = a$, we have a collision. The b that corresponds to $R_m = a$ gives the radius of a virtual sphere that placed at the location of our blue sphere in the absence of forces would absorb the same amount of particles.

Hence, the number of collisions in the presence of forces is:

$$J_f = \pi b^2 N c \tag{3.2.2}$$

and the enhancement factor is:

$$\boxed{E.F = \frac{b^2}{a^2}} \tag{3.2.3}$$

We will now see how to compute b.

As the force is a central force, the kinetic moment is conserved. At $r = R_m$ it is equal to $R_m v_{max}$ and far away, it is equal to $b v_\infty$. Remembering that $\frac{1}{2} m v_\infty^2$ is also the total energy of the particle E.

So we have:

$$b^2 = R_m^2 \frac{m v_{max}^2}{2E} \tag{3.2.4}$$

but from the conservation of energy we also have $U(R_m) + \frac{1}{2} m v_{max}^2 = E$, hence:

$$b^2 = R_m^2 \left[1 - \frac{U(R_m)}{E} \right] \tag{3.2.5}$$

By replacing $E = \frac{1}{2}mv_\infty^2$ by $\frac{3}{2}kT$ and R_m by a, we get the enhancement factor:

$$\boxed{E.F \;=\; 1 - \frac{2U(a)}{3kT}} \tag{3.2.6}$$

Remarks

Here we use the mean square speed to express the total energy of the particle. To be more precise, we should have averaged the E.F. over the complete Maxwellian distribution $f(v)$ of speeds:

The contribution to the total flux of the $dn = Nf(v)dv$ particles having speed between v and $v + dv$ being $dJ_f = \pi a^2 v E.F(v)dn$, we have:

$$dJ_f = \pi a^2 v E.F(v) N f(v) dv \tag{3.2.7}$$

$$\Rightarrow \quad J_f = \pi a^2 N \int_v v E.F(v) f(v) dv \tag{3.2.8}$$

$$\tag{3.2.9}$$

So that the mean enhancement factor is:

$$E.F_{mean} = \frac{1}{c}\int_v v E.F(v) f(v) dv \tag{3.2.10}$$

$$E.F_{mean} = 1 - \frac{U(a)}{c}\int_v \frac{f(v)}{\frac{1}{2}mv} dv \tag{3.2.11}$$

The enhancement factor is a non-dimensional property that does not depend on the frame of reference it is calculated in. Hence we do not need to modify it when moving to the absolute frame of reference.

3.2.2 Case of pure Coulombic interaction

Using the formula we just derived, we get:

$$E.F. \;=\; 1 + \frac{q_1 q_2}{4\pi\varepsilon_0 akT} \tag{3.2.12}$$

3.2.3 Case of pure image forces

In the case of a pure image force between a point charge and a neutral aerosol:

$$E.F. = 1+2\sqrt{\frac{1}{4\pi\varepsilon_0}\frac{\pi q^2}{8akT}} \tag{3.2.13}$$

3.2.4 Case of repulsive force

The above theory is only valid for an attractive force. In the case of a repulsive force, the idea is to say that the particles have to overcome an energy barrier $\psi(R_m)$ where R_m is the distance that maximizes the potential (in case of repulsive Coulombic force, $R_m = a$) and that only a proportion $e^{-\frac{\psi(R_m)}{kT}}$ of the particles will be able to overcome this barrier.

$$E.F. = e^{-\frac{\psi(R_m)}{kT}} \tag{3.2.14}$$

3.3 Correction in the intermediate regime

For the sake of simplicity we will only derive the formulas in the case of pure deposition (attractive potential) without evaporation from the surface of the absorbing particle

The correction's idea is the same as in the case without interaction: We introducing a boundary sphere around the absorbing particle. Outside this boundary sphere, the flux of particle is supposed to be driven by a continuous diffusion process, inside the boundary sphere, the flux is supposed to be in the free molecular regime and the two fluxes are set equal at the boundary. Applying this idea for a boundary sphere located at a distance δ from the surface gives:

Outer part $(r \geq a+\delta)$

$$J_c = \frac{4\pi D(N_\infty - N' e^{\frac{\psi(a+\delta)}{kT}})}{\int_\delta^\infty \frac{1}{r^2} e^{\frac{\psi(r)}{kT}}} \tag{3.3.1}$$

N' is the concentration at the distance δ from the absorbing sphere

Inner part $(a \leq r \leq a+\delta)$

$$J_f = \pi E.F.a^2 N' c = \pi b^2 N' c \tag{3.3.2}$$

Matching

By equating the two fluxes, we can eliminate N' and find the new expression of the flux.

$$\boxed{J = \frac{4\pi aD}{a\int_{a+\delta}^{\infty} \frac{1}{r^2} e^{\frac{\Phi(r)}{kT}} dr + \frac{4aD}{b^2 c} e^{\frac{\Phi(a+\delta)}{kT}}}} \tag{3.3.3}$$

And with the usual corrections:

$$\boxed{J = \frac{4\pi(a_1+a_2)(D_1+D_2)}{(a_1+a_2)\int_{a_1+a_2+\sqrt{\delta_1^2+\delta_2^2}}^{\infty} \frac{1}{r^2} e^{\frac{\Phi(r)}{kT}} dr + \frac{4(a_1+a_2)(D_1+D_2)}{b^2\sqrt{c_1^2+c_2^2}} e^{\frac{\Phi\left(a_1+a_2\sqrt{\delta_1^2+\delta_2^2}\right)}{kT}}}} \tag{3.3.4}$$

- We here made the implicit hypothesis that the boundary sphere diameter δ is larger than the minimum impact parameter b.
- Many potentials of interest are bigger than kT only in regions close to the particles, so that it might be possible to set $e^{\frac{\Phi(r)}{kT}} \simeq 1$ for $r \geq a+\delta$. If this approximation is possible the kernel becomes:

$$J = \frac{4\pi aD}{\frac{a}{a+\delta} + \frac{4aD}{b^2 c}} \tag{3.3.5}$$

$$\Rightarrow \quad J = \frac{4\pi aD}{\frac{a}{a+\delta} + \frac{4D}{E.F.ac}} \tag{3.3.6}$$

Which is the same as a formula with no potential but with a collision probability of $E.F > 1$

Chapter 4

Turbine and nozzle microphysics

Recent measurements have suggested that soot properties can evolve downstream of the combustor, changing the characteristics of aviation particulate matter (PM) emissions and possibly altering the subsequent atmospheric impacts. Microphysical processes and interactions with gas phase species have been modeled for temperatures and pressures representative of in-service engines. Time-scale arguments are used to evaluate the relative contributions that various phenomena may make to the evolution of soot, including coagulation growth, ion-soot attachment, and vapor condensation. Then a higher-fidelity microphysics kinetic model is employed to estimate the extent to which soot properties evolve as a result of these processes. Results suggest that limited opportunities exist for the modification of the size distribution of the soot, its charge distribution, or its volatile content, leading to the conclusion that the characteristics of the turbine and nozzle of an aircraft engine have little or no influence on aircraft non-volatile emissions. Combustor processing determines the properties of soot particulate matter emissions from aircraft engines, setting the stage for interactions with gaseous emissions and development as cloud condensation nuclei in the exhaust plume.

4.1 Introduction

Recent measurements have suggested that soot properties can evolve within an aircraft engine, altering the characteristics of the emitted PM [56] [35]. This chapter addresses the potential for the post-combustion thermodynamic environment to influence aircraft non-volatile, carbonaceous PM emissions. Measurements have demonstrated that exhaust gases and water vapor condense on emitted non-volatile particles in the exhaust plume [17][41]. This can change the tendency for non-volatile PM to act as cloud con-

densation nuclei and alter their role in contrail formation. Radiative forcing resulting from contrail and cirrus cloud formation has been indicated by measurements [49] and the cumulative magnitude of the effect to date is estimated to be roughly equivalent to that of carbon dioxide emissions from aviation [3][40],[24],[25],[27],[31]. Heterogeneous processing may also influence the chemical composition of aircraft soot emissions with potential toxicological consequences. It is currently unknown whether non-volatile, carbonaceous PM should be classified as a hazardous air pollutant (HAP) [51]. Apart from the classification of the soot itself, it is also possible that the soot could absorb or act as a condensation site for other emitted HAPs. Since condensation on non-volatile PM is partly controlled by the particle size distribution, it is important to understand the potential for coagulation growth within and downstream of the engine. Understanding differences in non-volatile particle properties at the combustor exit relative to their subsequent state at the engine exit may also improve the combustor development process. As measurement capabilities for determining particle emissions are matured and implemented, knowing that the combustor exit plane is a viable alternative measurement location to the engine exit plane can save considerable expense in sampling. Experimental programs, including the NASA-QinetiQ Collaborative Program [56] and the European Union PartEmis project [35], have begun to investigate potential modification of soot properties through the engine turbine and exhaust nozzle. A limited number of these measurements show significant changes in the non-volatile size distribution and the presence of volatile condensate on the soot. Whitefield et al. [56] report a 3 nm (10%) growth in particle mean diameter. This increase may indicate that intra-engine thermodynamic conditions are favorable for coagulation or condensation. Petzold et al. [35] also measure an increase in the mean diameter, but attributed the change to variability in engine operating point between experiments rather than an active microphysical process. In addition, Petzold et al. [35] detected a volatile coating on soot particles at the engine exit that was not evident on particles at combustor exit. These different interpretations of the measured particle growth were one impetus for the model development and analysis of this study. While we treat the intra-engine environment specifically, it is important to note that results developed through both the NASA-QinetiQ and PartEmis programs were perhaps confounded by the possibility of additional heterogeneous processing within the particulate measurement systems themselves. There is a strong modification in the pressure and temperature environment experienced by the particle after entering the sampling probe. This is coupled with a time-scale within the apparatus that is longer than the absolute age of the soot particle at the time it enters the probe. This study employs numerical models and time-scale analyses to explore the potential for soot particle growth via agglomeration, particle scavenging, and vapor condensation in the engine turbine and nozzle. Several studies have addressed the evolution of the chemical state of the flow through the turbine and nozzle of an aircraft engine [7][23][29][46][50][57][22].

These investigations have shown the unique role of gas phase chemistry along the post-combustion flow path in the production of sulfate and nitrate aerosol precursors. Little is known about the evolution of non-volatile PM through this same environment. Estimates of precursor emissions suggest that non-volatile particulate emissions constitute a major fraction of the total particulate mass found in the near-field plume (1s after emission) [22]. Soot is the only component of the overall PM mass present at these times that has nucleated and developed by the combustor exit and is the dominant contributor to aircraft engine non-volatile emissions, representing virtually all the non-volatile particle mass. Rates for the microphysical processes that govern the evolution of non-volatile PM can be determined with the knowledge of the temperature and pressure of the surrounding environment and the initial chemical composition of the fluid. After formation in the primary zone of the combustor, soot particles undergo rapid coagulation and surface growth, and are cooled through the addition of dilution air in the combustor aft section. By the time particles arrive at the turbine inlet, their mean age is on the order of 3-8 ms and they are at a temperature 500-1000 K lower than at nucleation. At ground level, the particles undergo a fast expansion through the turbine and nozzle from pressures as high as 40 atm for in-service engines to atmospheric pressure within 1-3 ms. The flow is also diluted by the addition of turbine cooling air early in the gas path (cooling can be responsible for more than 20% of the mass flow) and later again in the nozzle for engines with internal core-bypass mixing. This paper is organized to provide a step-by-step description of the analysis of this intra-engine system. In Section 1 we examine the evolution of the soot size distribution due to coagulation between neutral particles. Section 2 deals with the charge distribution and its effect on the coagulation. Section 3 summarizes conclusions from our evaluation of the potential for non-volatile particulate matter processing in the post-combustor flow path within a gas turbine engine

4.2 Coagulation

In this section we consider coagulation as a means for particle growth within the engine. Three types of coagulation have been considered: Brownian coagulation, turbulent shear coagulation, and turbulent inertial coagulation. In most flows and for most particle types, Brownian coagulation is dominant. However, since the flow in an aircraft turbine is strongly turbulent, it was not clear at the outset whether the two latter types of coagulation would be negligible within the engine. A bounding analysis shows this to be the case for turbomachinery flows and the particle size ranges expected in an aircraft engine. The evaluation also suggests that any intra-engine coagulation that occurs will be confined to the combustor. We first examine characteristic time-scales for coagulation to assess whether there is enough time within the engine for such processing to occur.

Characteristic time-scales are estimated as $\frac{2}{K_c N_0}$, where N_0 is the particle number density at the beginning of the coagulation process and K_c is the coagulation kernel. The coagulation kernel is the equivalent of a chemical reaction rate parameter. The nomenclature differs simply to reflect the non-chemical nature of the process but it refers to the same concept. Strictly, coagulation time-scales are properly defined only for monodisperse distributions, but we still can define the time-scale here as an upper bound for the time necessary to decrease the particle number density by a factor of 2. Soot radii between 5 nm and 50 nm were considered, matching the range found in existing measurements of non-volatile particulate emissions from aircraft engines [20] [42] [1] [6] [11] [28] [37] [2]. To estimate N_0, further specification of soot properties such as the mass emission index and the size distribution is required. At the combustor exit of aircraft engines, soot has been measured to be log-normally distributed in a single mode (e.g. [56]). For this analysis, we assess an upper bound on the amount of coagulation that may occur using a large central size and geometric standard deviation. Coagulation kinetics are driven by N_0. The total mass of non-volatile PM is specified using an emission index for soot, EIPMnv, of 1 g/kg_{fuel}. This is likely on the high end for the range of engines in service. Assuming a soot density between 1500-1800 kg/m^3, and using lognormal parameters suggested by measurements [20] [42] [1] [6] [11] [28] [37] [2]- median radius in the range 10-30 nm, geometric standard deviation 1.5-1.75, and number EI of 0.1E15-6E15 particles/kg_{fuel} data suggest EIPMnv is in the range 0.002-2 g/kg_{fuel}. For this study, the log-normal distribution of this mass is specified by a median radius of 23 nm and a geometric standard deviation of 1.75. Both of these values are on the high end of the range suggested by existing measurements. The choice of a large emission index and particle size is meant to put the system in a worst-case scenario for kinetics. The mass density of the soot was assumed at 1.5 g/cm^3. Integrated, the reference distribution equates to a number density of soot particles in the range 3E8-5E8 $/cm^3$ at combustor exit conditions that will be used as N_0. Coagulation kernels can be rigorously derived for spherical particles, which is an assumption we are making for aircraft soot. However, the morphology of aircraft soot is still an area of active research. Other kinds of soot particles, such as those created by automobiles, would poorly fit into such a model. Knowledge of temperature and pressure is sufficient to compute the coagulation kernel. The Brownian coagulation kernel is computed according to Fuchs [28] as given in Eq. (1) for two colliding particles.

$$K_{c_{br}} = \frac{4\pi * (r_1 + r_2) * (D_1 + D_2)}{\frac{(r_1+r_2)}{(r_1+r_2)+\sqrt{\delta_1^2+\delta_2^2}} + \frac{4*(D_1+D_2)}{\sqrt{c_1^2+c_2^2}(r_1+r_2)}} \quad (1) \qquad 4.2.1$$

In Eq. (1), r is the particle radius and δ is the final mean free path distance between

the 2 particles just before their collision as derived by Fuchs [9] and shown in Eq. (2). In Eq. (2), λ_a is the apparent mean free path of the particle in the carrier gas as given by Eq. (3).

$$\delta = \left[\frac{1}{6r\lambda_a}\left((2r+\lambda_a)^3 - \left(4r^2+\lambda_a^2\right)^{\frac{3}{2}}\right) - 2r\right] \quad (2) \qquad 4.2.2$$

$$\lambda_a = \frac{kTC_c}{c3\pi\mu r} \qquad 4.2.3$$

(3)

Referring to Eq. (1), c is the particle mean speed as given in Eq. (4), where m is the particle mass, and D is the particle diffusivity as in Eq. (5), where C_c is an empirically derived function as given in Eq. (6).

$$c = \left(\frac{8kT}{\pi m}\right)^{\frac{1}{2}} \qquad 4.2.4$$

(4)

$$D = \frac{kTC_c}{6\pi\mu r} \qquad 4.2.5$$

(5)

$$C_c = 1 + \frac{\lambda}{r}\left[1.257 + 0.4e^{-\frac{1.1r}{\lambda}}\right] \qquad 4.2.6$$

(6)

In Eq. (6), C_c corrects for the non-continuum effects at low gas densities and small particle radius [43]. In Eq. (6), λ is the mean free path of the carrier gas as given in Eq. (7), where μ is the dynamic viscosity of air given by Sutherland's law given in Eq. (8).

$$\lambda = \frac{2\mu}{P\left(\frac{8}{\pi}\frac{M}{RT}\right)^{\frac{1}{2}}} \qquad 4.2.7$$

(7)

$$1.7894.10^{-5} * \left(\frac{T}{273.11}\right)^{\frac{3}{2}} \frac{273.11 + 110.56}{T + 110.56} \qquad 4.2.8$$

(8)

Referring back to Eq. (1), β is the sticking probability, the probability that a collision will result in coagulation, and it is set to one in the rest of this analysis to correspond to an upper-bound scenario. The turbulent shear coagulation kernel was calculated according to Saffman and Turner [39] as given in Eq. (9).

$$K_{c_{tsh}} = 1.3(r_1 + r_2)^3 \left(\frac{\epsilon}{\nu}\right)^{\frac{1}{2}} \qquad 4.2.9$$

(9)

In Eq. (9), ν is the kinematic viscosity and ϵ is the dissipation rate, here approximated by the turbulence scaling law given in Eq. (10),

$$\epsilon = \frac{(rms * U)^3}{l} \qquad 4.2.10$$

(10)

In Eq. (10), U is the mean speed of the flow, L is the characteristic length scale for turbulent eddies, and rms is the root mean square turbulent intensity. To evaluate a maximum value for ϵ, we took U at $600m/s^{-1}$, approximately Mach 1 at engine nozzle exit temperatures, L at a typical blade thickness of 1 cm, and the rms of the turbulence at 20% based on the measurements in Goebel [10]. The turbulent inertial coagulation kernel was estimated according to Pruppacher and Klett [36] as given in Eq. (11).

$$K_{c_{tin}} = 5.7(r_1 + r_2)^2 \mid \frac{C_{c1}m_1}{6\pi\mu r_1} - \frac{C_{c2}m_2}{6\pi\mu r_2} \mid \left(\frac{\epsilon^3}{\nu}\right)^{\frac{1}{4}} \qquad 4.2.11$$

(11)

Computations of the three coagulation kernels (Eqs. (1), (9), (11)) can be found in Figures 1 to 5. These figures show the pressure-temperature dependence at fixed radius and the radius-radius dependence at fixed temperature and pressure of the three coagulation kernels. To examine the pressure-temperature dependence we fix the radii of the 2 colliding particles at the median radius of the distribution, 23 nm, and let the temperature and

pressure vary from 300 to 1900 K and 0.5 to 37 atm respectively. For the radius-radius dependence we fix the temperature and pressure at respectively 900 K and 10 atm and let the radii of the 2 colliding particles vary from 5 to 50 nm. Coagulation time-scales based on these estimates for K_c shown in Table 1 are 2 orders of magnitude larger than the residence times through the post-combustor flow path at the combustor exit. The conclusion is that there is little opportunity for coagulation through the turbine and exhaust nozzle, particularly since we have assumed a worst-case scenario for the kinetics. Note that a characteristic time-scale cannot be defined for turbulent inertial coagulation since it is by definition infinite for particles having the same radius. Thus, to assess the importance of turbulent inertial coagulation, compare the kernel values in Figures 2 and 5 and note they are of similar magnitude.

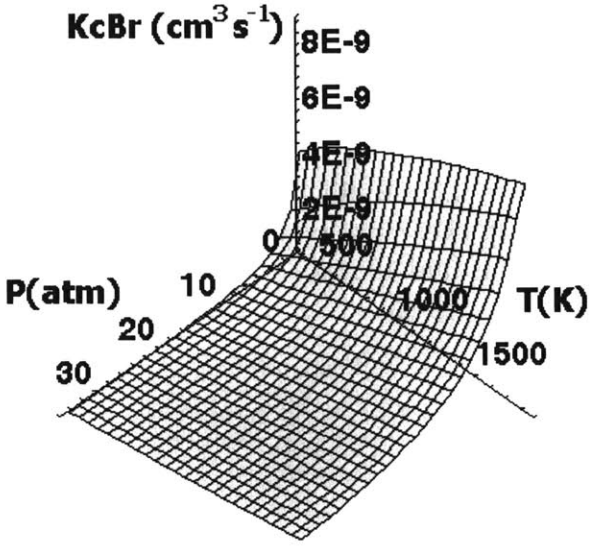

Figure 4.1: Temperature and Pressure dependance of Brownian coagulation kernel for two particles of soot having 23nm of diameter

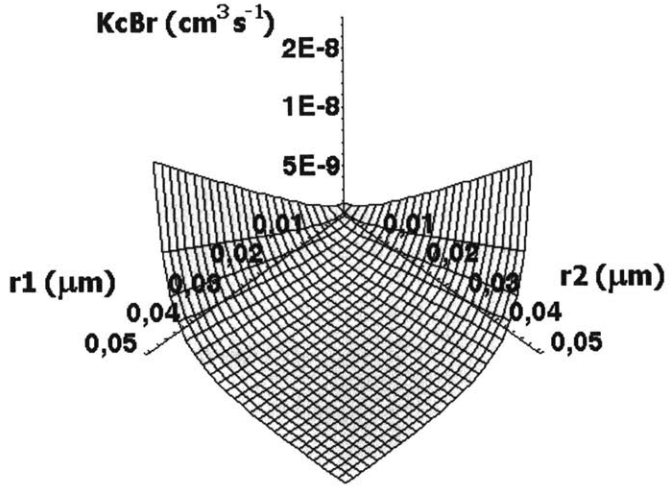

Figure 4.2: Radius dependance of Brownian coagulation kernel at 900 Kelvins and 10 Atm

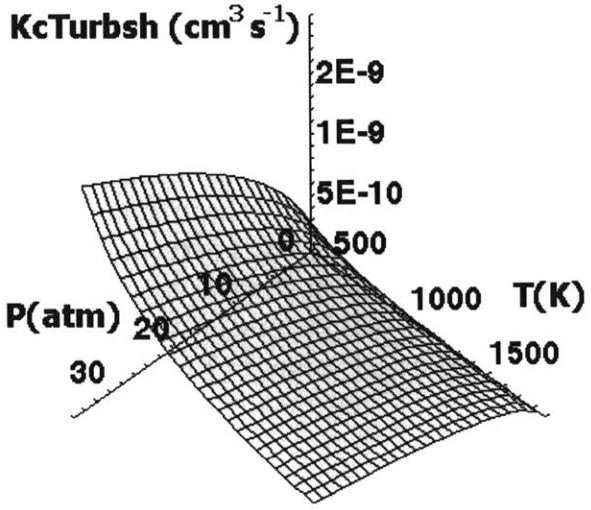

Figure 4.3: Temperature and Pressure dependance of turbulent shear coagulation kernel for two particles of soot having 23nm of diameter

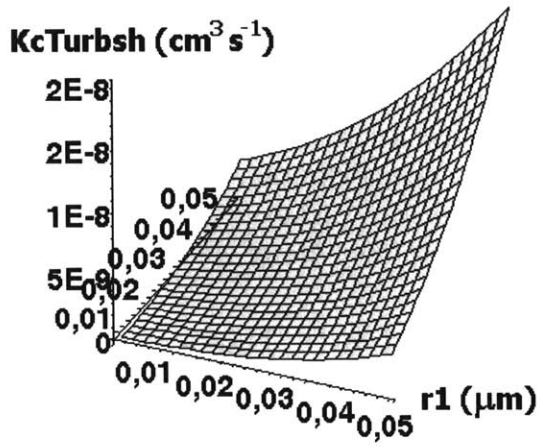

Figure 4.4: Radius dependance of turbulent shear coagulation kernel at 900 Kelvins and 10 Atm

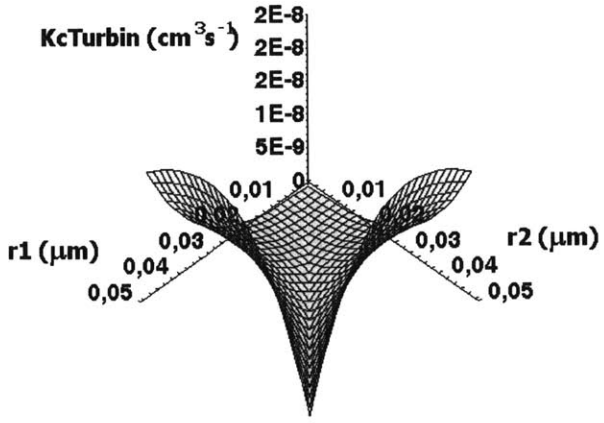

Figure 4.5: Radius dependance of turbulent shear coagulation kernel at 900 Kelvins and 10 Atm

As a consistency check, Table 1 also shows a time-scale relevant to a 5 nm radius,

monodisperse distribution of soot at an EI of 1 g/kg-fuel. This represents the condition in the combustor primary zone immediately after nucleation. We would expect that coagulation time-scales for this distribution would indicate that coagulation occurs within the combustor and the time-scale analysis correctly predicts this. If all the soot mass is concentrated into particles of 5 nm of radius, the time-scale for coagulation becomes 1 ms, which is shorter than typical combustor residence times.

	Reference distribution	Monodisperse distribution at 5 nm of radius
Brownian coagulation time-scale	200 ms	1 ms
Shear coagulation time-scale	500 ms	20,000 ms
Inertial coagulation time-scale	similar to Brownian time	virtually infinite
Turbofan combustor flow time-scale	5-8 ms	5-8 ms
Turbofan turbine flow time-scale	2-5 ms	2-5 ms

Table 1. Time-scale for coagulation process at combustor exit conditions versus typical residence time for particles.

A higher-fidelity analysis further confirms the conclusions derived from the time-scale comparisons. We modified the chemical library CHEMKIN coupled with the differential equations system integrator VODE to integrate the system of equation governing the concentrations of the microphysical species as differentiated by size. For the numerical analysis, the reference distribution previously described was discretized into 45 bins, truncated at a lower-bound radius of 5 nm, the likely minimum soot spherule size, and at the upper-bound of 500 nm, a size at which particles are almost non existent. The results of the integration through the turbine and exhaust nozzle enable us to assess changes in the median or geometric standard deviation. Figure 6 shows the particle concentration in the 45 bins at 4 locations through the turbine. Particle growth would be shown by an increase of the median diameter, a shift to the right of the distribution peak. However, coagulation growth is so weak that the simulation shows no shift within the numerical accuracy of the code. The only effect shown is due to the gas expansion through the turbine which lowers the number density by an order of magnitude.

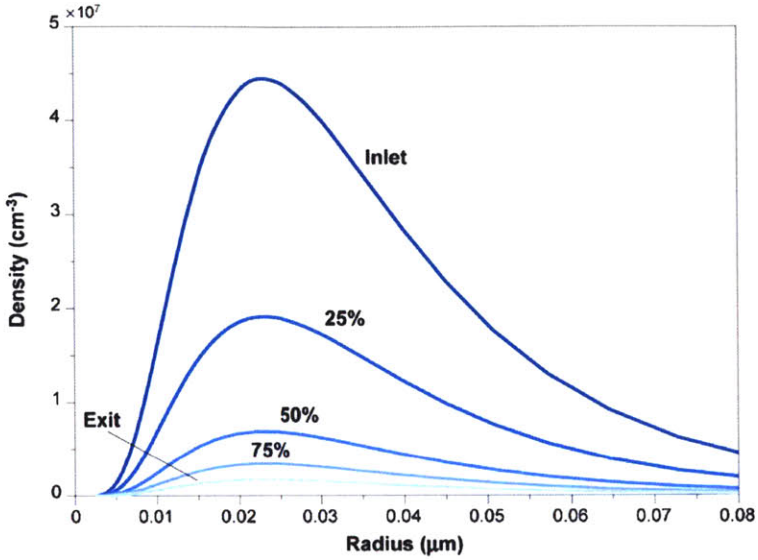

Figure 4.6: Simulated evolution of density versus radius through the turbine and nozzle at 5 locations.

4.3 Electrical State

Assessing electrical interactions is important for two reasons. First, in order to accurately characterize downstream plume processing of particles, the electrical state at the engine exit must be defined. Second, soot charges can increase the effective value of the coagulation kernel. To calculate an enhancement factor on the coagulation kernel, we need to estimate the non-volatile particle charge distribution as established within the combustor. Depending on the fuel type, the density of ions can be as high as 1E10-1E11 in the flame zone of the combustor [8]. Figure 7, reproduced from Ball and Howard [5], shows results from a thermoionization calculation suggesting that soot particles are positively charged at typical primary zone temperatures. However, once the soot leaves the flame front in the primary zone, electrons, which have a diffusion constant 3 orders of magnitude higher than any other charged particles present in the flow, should quickly ionize other species and disappear [44].

Following the disappearance of the free electrons will be a pool of positive and negative ions that have similar diffusion constants. These ions will recombine and attach to non-volatile particulates, altering the charge distribution of the soot. As shown in Figure 8, the ion-aerosol attachment coefficient, computed according to Hoppel and Frick [13] as

in Eq. (12), is of the same order of magnitude as the ion-ion recombination coefficient. Therefore the ions, which in the flame have a concentration at least three orders of magnitude larger than the soot particles, will have sufficient time to modify the charge distribution before they disappear.

$$K = \frac{4\pi r D_{ion}}{r\int_{\delta}^{\infty}\frac{1}{\rho^2}e^{\frac{\Phi(\rho)}{kT}}d\rho + \frac{4D_{ion}r}{cb^2}e^{\frac{\Phi(\rho)}{kT}}} \quad 4.3.1$$

(12)

In Eq. (12), D_{ion} is the ion diffusion constant, Φ is the potential between the ion and the soot particle, and δ is the final mean free path distance between the 2 particles just before their collision given by Eq. (13).

$$\delta = \frac{r^3}{\lambda_i^2}\left(\frac{2}{10}\left(1-\frac{\lambda_i}{r}\right)^5\right) - \frac{1}{3}\left(1+\left(\frac{\lambda_i}{r}\right)^2\right) * \left(1+\frac{\lambda_i}{r}\right)^3 + \frac{2}{15} * \left(1+\left(\frac{\lambda_i}{r}\right)^2\right)^{\frac{5}{2}} \quad 4.3.2$$

(13)

In Eq. (13) λ_i is the mean free path of the ions

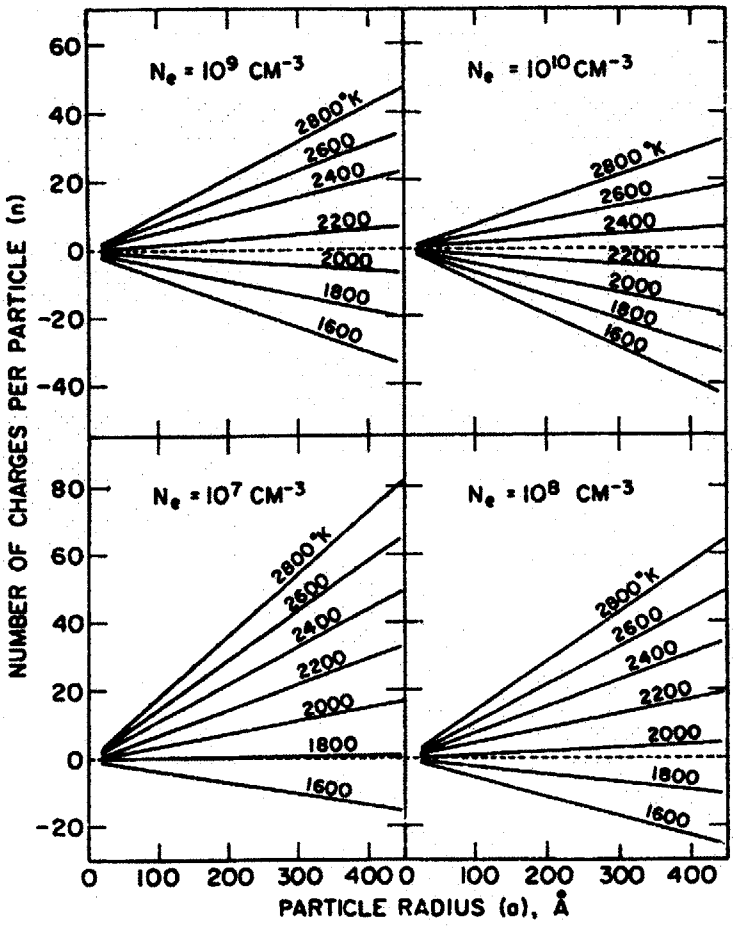

Figure 4.7: Equilibrium number of charges carried by soot particles depending on radius and number of free electron in the surrounding environment. Reproduced from Ball and Howard [5]

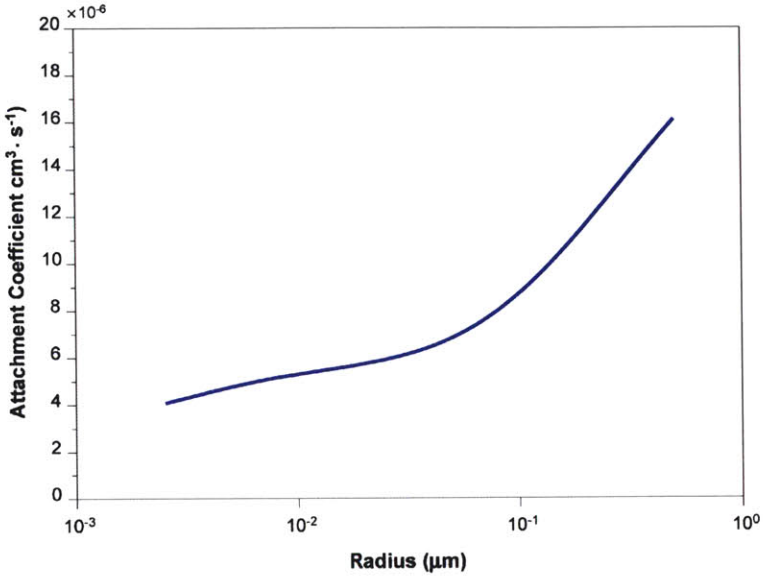

Figure 4.8: Ions-aerosol attachment coefficient at 1250 K for a soot particle bearing one charge and an ion bearing a charge of opposite polarity

In Eq. (12), b is the minimum impact parameter leading to a collision, obtained by minimizing the function in Eq. (14) with respect to ρ

$$b(r) = \rho^2 \left(1 - \frac{2\Phi(\rho)}{3kT}\right) \qquad 4.3.3$$

(14)

The ion diffusion constant is computed from the ion mobility. The mobility of an ion (as distinct from free electrons) is about 1 $cm^2/V - s$ [8]. We assumed a mobility of $1.2cm^2/V - s$ for our analysis and a mass of 100 AMU for both positive and negative ions [12]. Our calculations show that because of the small radius of an ion, image and Van der Walls forces are negligible compared to Coulombic forces and hence we have neglected them. To evaluate the evolution of the charge distribution, the ion-ion recombination coefficient is parameterized over the range 1E-8 to 1E-5 cm3-s-1. Experimental results suggest that the lower end of this range is more likely [36,38]. Figure 9 shows the evolution of the relative concentrations of soot particles with -2, -1, 0, +1, and +2 charges when the initial ion concentration is 1E11 cm^{-3} and the ion recombination rate is 1E-7 $cm^{-3}s{-}1$. It demonstrates rapid convergence to a steady state charge distribution

of the soot particles. This result varies little over the range of ion-ion recombination rates examined, showing a difference only at the highest values. Indeed, the higher the ion-ion combination rate the less the soot charge distribution will evolve and the more dominant one polarity will be. For aircraft combustors this would lead to positively charged soot. However, our results suggest that the ions indeed have sufficient time to set the charge distribution of the soot. Moreover, the speed at which the convergence takes place indicates that the steady-state is attained within the combustor. The practical conclusion is that, if the ion concentration is sufficiently large and the attachment coefficient sufficiently fast (which are probable conditions in the combustor), then the charge distribution would be such that a significant proportion of the soot particles are carrying opposite charges. Thus, there is a potential for increased coagulation due to electrical interactions between oppositely-charged particles. Coagulation enhancement occurs when there is an attractive potential between particles. We consider Coulomb forces, image forces (which are a correction to the Coulombic interaction), and Van der Walls forces. The Van der Walls potential between two particles separated by a distance ρ is computed according to Eq. (15).

$$\Phi_{vdw}(\rho) = -\frac{A_H}{6}\left[\frac{2r_1r_2}{\rho^2-(r_1+r_2)^2}+\frac{2r_1r2}{\rho^2-(r_1-r_2)^2}+ln\left(\frac{\rho^2-(r_1+r_2)^2}{\rho^2-(r_1-r2)^2}\right)\right] \quad 4.3.4$$

(15)

In Eq. (15), A_H is the Hamaker constant with a value of 5E-20 J [15][30]. The sum of the Coulombic and image forces is computed as given by Maxwell [26] in Eq. (16). In Eq. (16), ϵ_r is the relative permittivity of the soot particle taken as 5.5 [14].

$$\Phi_C(\rho) = -\frac{q^2}{8\pi\varepsilon_0}\frac{\varepsilon_r-1}{\varepsilon_r+1}\left((p_{11}-\frac{1}{r_1})q_1^2+2p_{12}q_1q_2+(p_{22}-\frac{1}{r_2})q_2^2\right) \quad 4.3.5$$

(16a)

$$p_{ii}=\frac{b_{jj}}{b_{ii}b_{jj}-b_{ij}^2} \qquad p_{ij}=-\frac{b_ij}{b_{ii}b_{jj}-b_{ij}^2} \quad 4.3.6$$

(16b)

$$b_{ii}=r_i(1-\eta_{ij})\sum_{m=0}^{\infty}\left[\frac{\theta^m}{1-\eta_{ij}\theta^{2m}}\right] \qquad b_{ij}=-(\frac{r_ir_j}{r})(1-\theta^2)\sum_{m=0}^{\infty}\left[\frac{\theta^m}{1-\theta^{2m+2}}\right] \quad 4.3.7$$

(16c)

$$\eta_{ij} = \left[\frac{r_i + \theta r_j}{\rho}\right]^2, \quad \theta = \gamma - \sqrt{\gamma^2 - 1}, \quad \gamma = (\frac{\rho^2 - r_i^2 - r_j^2}{2 r_i r_j} \qquad 4.3.8$$

(16d)

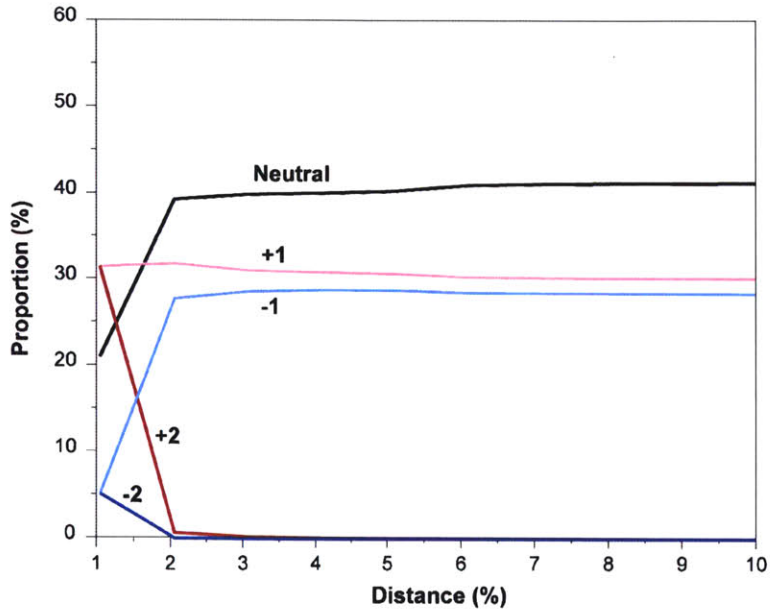

Figure 4.9: Evolution of the proportion of soot particles bearing -2, -1, 0, +1, and +2 charges in the turbine starting from an arbitrary (here positive) charge distribution with an ion concentration of $1.10^{11} cm^{-3}$ and an ion recombination rate of $1.10^{-7}\ cm^{-3} s^{-1}$.

As with the previous consideration of the initial soot charge distribution, the enhancement to the kernel is represented as an increase in the minimum impact parameter leading to a collision, given in Eq. (14). Equation (17) is the revised kernel, including enhancement.

$$J = \frac{4\pi(a_1+a_2)(D_1+D_2)}{\frac{a_1+a_2}{a_1+a_2+\sqrt{\delta_1^2+\delta_2^2}} + \frac{4(a_1+a_2)(D_1+D_2)}{b^2\sqrt{c_1^2+c_2^2}}} \qquad 4.3.9$$

(17)

The enhancement to the kernel, i.e. the factor by which the kernel is increased when the electrical state of the particles is considered, is plotted on Figure 10 as a function

of the radius of the 2 colliding particles. It shows that due to the high temperature and the relatively large size of the soot particles, the enhancement factor will remain of the order of one, hence having only a negligible effect on the coagulation. Integration of the soot distribution using the higher fidelity microphysical tool confirms the lack of growth through the turbine and exhaust nozzle for the range of conditions investigated.

4.4 Role of hydrocarbons in altering soot properties

As a final step, we briefly consider the potential for hydrocarbons (HC) to play a role in altering particle properties. Emission indices for unburned HCs can be of the same order of magnitude as the non-volatile particulate EI [16]. Thus, if condensation occurs, it could modify the particle mass and hence size distribution. Analyses of plume measurements have, however, suggested the presence of HC nucleation in the plume [35] [6] [58] [19]. However, saturation vapor pressures of these gaseous emissions are quite high under the temperature and pressure conditions experienced in the turbine flow. Using the Antoine's Law coefficients reported in [52] a few examples are computed and listed in Table 2 for HC species that might be found at the combustor exit [45]. Gas phase species at the combustor exit include organics such as small hydrocarbons and aldehydes, aromatics and substituted aromatics, and to a lesser extent, larger hydrocarbons.

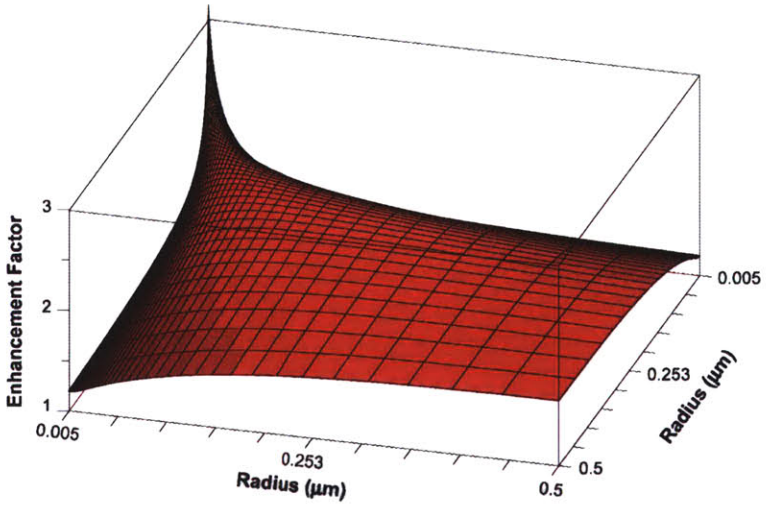

Figure 4.10: Enhancement factor at 1250K between two particles bearing respectively -1 and +1 charge respectively.

Heptadecane (500 K)	1-decene (440 K)	1-methyl-naphthalene (500 K)	Benzaldehyde (440 K)
0.15atm	0.91atm	0.67atm	0.74 atm

Table 2. Saturation pressures of some species at temperature given in parenthesis.

To our knowledge, no existing measurements at the engine exit detail the speciation of the hydrocarbons with carbon number higher than 17. In general, however, the saturation vapor pressures for the conditions examined suggest that condensation of hydrocarbons in the engine or even the near-field plume is not expected. Plume measurements may instead point to other organic emissions such as droplets of engine lubricating oil or other high carbon number compounds. This discussion of condensation does not address the gas-to-particle conversion in the exhaust flow after it exits the engine or as an exhaust sample is captured by a measurement probe and transported to a measurement instrument where temperatures and pressures may change dramatically. An additional effect not addressed here is the stabilization of hydrocarbon monolayers on the surface of the soot, which can be enhanced in the presence of (positive) charges [58]. This particular kind of deposition could potentially lead to a growth of the particle even at sub-saturated conditions. In the absence of charges, monolayers only influence the chemical properties of the non-volatile particulate without modifying the microphysical properties.

4.5 Summary

We considered the post-combustion evolution of soot properties within an aircraft engine through coagulation as potentially enhanced by electrical interactions. No process was identified that would lead to a change in soot size or charge distribution through the turbine and nozzle of the engine. The formation and initial evolution of the soot happens in the combustor. Cooling and dilution through the combustor dilution zone, turbine, and exhaust nozzle essentially freezes the properties of the non-volatile particulate matter prior to emission. Thus, we conclude that combustor exit measurements are representative of engine exit measurements, and that changes in size distribution measured in recent sampling programs [56][35] are likely related to changes in experimental conditions, including variance in engine operating conditions, or additional processing through the measurement apparatus. It should be emphasized that these results are relevant only to the non-volatile particulate. Gas phase species do evolve significantly through the post-combustion gas path.

Chapter 5

Homogeneous Nucleation

The work in this chapter is based on [36],[43],[18],[47],[55],[33],[34],[53],[54],[21],[48].

Nucleation is the process through which a gaseous phase merges to form a solid or liquid phase. If the process does not involve a foreign surface, the nucleation is said to be **homogeneous**. On the other hand, if the process involves a foreign surface (mist on a bathroom's mirror) the nucleation is said to be **heterogeneous**.

The other important notion is the distinction between **homomolecular** and **heteromolecular** nucleation, the former involves gas molecules of only one chemical species, the latter involves gas molecules of more than one species. If the number of species is 2, we also use the term **binary** nucleation

5.1 A few useful relations

5.1.1 Mechanical equilibrium between two phases separated by a curved surface

Surface tension theory tells us that at a point on a curved surface, one is able to find two directions of extremal radius of curvature (R_1 and R_2) and that the pressure drop across the interface is:

$$\Delta p = \sigma\left(\frac{1}{R_1}+\frac{1}{R_2}\right) \tag{5.1.1}$$

Where σ is the surface tension.

5.1.2 Chemical equilibrium between two phases separated by a curved surface. Gibbs-Helmotz Equation

We note $\mu(p,T,a) = \mu_0(p,T) + kTln(a)$ the chemical potential of a molecule in a phase of activity a.

We derive one of the Gibbs-Helmoltz equations:

$$d\left(\frac{\mu}{T}\right) = \frac{\partial}{\partial T}\left(\frac{\mu_0}{T}\right)dT + \frac{\partial}{\partial p}\left(\frac{\mu_0}{T}\right)dp + kdln(a) \quad 5.1.2$$

$$d\left(\frac{\mu}{T}\right) = \frac{1}{T}\left(-s_0 - \frac{\mu_0}{T}\right)dT + \frac{v_0}{T}dp + kdln(a) \quad 5.1.3$$

$$d\left(\frac{\mu}{T}\right) = \frac{1}{T}\left(-s_0 - \frac{\mu_0}{T}\right)dT + \frac{v_0}{T}dp + kdln(a) \quad 5.1.4$$

$$d\left(\frac{\mu}{T}\right) = -\frac{h_0}{T^2}dT + \frac{v_0}{T}dp + kdln(a) \quad 5.1.5$$

v_0 is the volume occupied of a molecule. h_0 is the enthalpy of a molecule.

Let us consider a gas phase $'$ and a condensed phase $''$ at the same temperature ($dT = 0$). The condensed phase is spherical (radius R_p) and surrounded by a large amount of gas phase. Chemical equilibrium between those two phases can be written as:

$$d\left(\frac{\mu'}{T}\right) = d\left(\frac{\mu''}{T}\right) \quad 5.1.6$$

$$\Longrightarrow \quad \frac{v_0'}{T}dp' - \frac{v_0''}{T}dp'' + kdln\left(\frac{a'}{a''}\right) = 0 \quad 5.1.7$$

$$\Longrightarrow \quad \frac{v_0'-v_0''}{T}dp' - \frac{v_0''}{T}d(p''-p') + kdln\left(\frac{a'}{a''}\right) = 0 \quad 5.1.8$$

$$\Longrightarrow \quad \frac{v_0'-v_0''}{T}dp' - \frac{v_0''}{T}d\left(\frac{2\sigma}{R_p}\right) + kdln\left(\frac{a'}{a''}\right) = 0 \quad \text{(Mechanical equilibrium)} \quad 5.1.9$$

Now, the gas phase is assumed to be large in extent so that $dp' \simeq 0$ during an infinitesimal evolution of the system, so that:

$$\boxed{-\frac{v_0''}{T}d\left(\frac{2\sigma}{R_p}\right) + kdln\left(\frac{a'}{a''}\right) = 0} \quad (5.1.10)$$

This equation will enable us to find a relation between the saturation pressure over a flat surface $R_p = \infty$ and the saturation pressure over a surface of radius R_p. The activity a'' of the condensed phase is equal to one. The volume v_0'' occupied by a molecule in

the condensed phase is held constant (incompressible condensed phase). So the above relation only depends on a' and R_p. Integrating it between R_p and ∞ we get:

$$\frac{a'_{eq,radius=R_p}}{a'_{eq,radius=\infty}} = e^{\frac{2v_0''\sigma}{kTR_p}} \tag{5.1.11}$$

The activity in the gas phase being the partial pressure divided by the overall pressure, we finally have:

$$\boxed{P_{sat,R_p} = P_{sat}e^{\frac{2v_0''\sigma}{kTR_p}}} \tag{5.1.12}$$

Where we simply define P_{sat} as the saturation pressure over a flat surface.

This relation is called the **Kelvin equation**. It tells us that, for a droplet of radius $R_p \neq \infty$ to be at equilibrium with its surrounding environment, the gas partial pressure has to be greater than the saturation pressure.

We can rearrange this equation to derive the equilibrium radius R_p of a droplet when the surrounding partial pressure of gas is P_{part} and the saturation ratio is $S = \frac{P_{part}}{P_{sat}}$:

$$\boxed{R_p = \frac{2v_0''\sigma}{kTln(S)}} \tag{5.1.13}$$

5.2 Thermodynamics: critical size and composition

5.2.1 Homomolecular nucleation

Statistical description of the system

Homogeneous homomolecular nucleation of a species A occurs when the saturation ratio $S = \frac{p_A}{p_A^s(T)}$ of the species A is greater than 1. (p_A is the partial pressure of A; $p_A^s(T)$ is the saturation vapor pressure of A above a flat surface)

Indeed at $S = 1$, an instantaneous snapshot would reveal that nearly all molecules of A are independent or in small clusters containing two, three or maybe four molecules. Larger clusters would be extremely rare and unstable.

When the saturation ratio becomes strictly greater than 1, we have an excess amount of vapor molecules. This excess bombards the clusters so that some of them might be able

to reach the critical stable size given by Kelvin equation ($R_p = \frac{2v_0''\sigma}{kTlnS}$) at which they won't shrink anymore.

The nucleation rate is the number of clusters that reach this critical size per unit time.

Let's consider a system composed of a total of N_{tot} molecules (free gas molecules + molecules inside the clusters)

Let us call N_a the number of clusters composed of a molecules of A. The Helmotz free energy of a cluster of $a > 1$ molecules is:

$$G_a = \left[a\mu_p + \sigma\Omega_a + kTln\frac{N_a}{N_{tot}}\right] \quad 5.2.1$$

The first term on the right hand side, μ_p, is the free energy of a molecule in the particle (condensed phase). The second term on the right hand side is the energy necessary to create an interface of surface Ω_a when the surface tension is σ.

This being the free energy of the clusters of size a the total free energy of the system is:

$$G = \sum_{a\geq 1} N_a G_a \quad 5.2.2$$

At equilibrium we must have:

$$\delta G_{T,P} = 0 \quad 5.2.3$$

We notice that the Gibbs-Duhem relation simplifies $\delta G_{T,P}$ to:

$$\delta G_{T,P} = \sum_{a\geq 1} G_a \delta N_a \quad 5.2.4$$

$$\delta G_{T,P} = \mu_v \delta N_1 + \sum_{a\geq 2}\left[a\mu_p + \sigma\Omega_a + kTln\frac{N_a}{N_{tot}}\right]\delta N_a \quad 5.2.5$$

This equation is subject to the following conservation equation:

$$N_1 + \sum_{a\geq 2} aN_a = N_{tot} \quad 5.2.6$$

We replace δN_1 in the last equation using $\delta N_1 + \sum_{a\geq 2} a\delta N_a = 0$:

$$\sum_{a\geq 2}\left[-a\mu_v + a\mu_p + \sigma\Omega_a + kTln\frac{N_a}{N_{tot}}\right]\delta N_a = 0 \qquad 5.2.7$$

$$\boxed{N_a = N_{tot}e^{-\frac{a(\mu_p-\mu_v)+\sigma\Omega_a}{kT}}} \qquad (5.2.8)$$

The numerator of the exponent can be interpreted as the energy required in order to form an single cluster of size a.

Let us denote ΔG as this energy.

$$\Delta G = a\left[\mu_p(P_p) - \mu_v(P_v)\right] + \sigma\Omega_a \qquad 5.2.9$$

where we have specified the pressures. Indeed, μ_p is taken at the pressure in the particle whereas μ_v is at the pressure in the vapor.

Energetics of the cluster

In the last part we showed that: $\Delta G = a\left[\mu_p(P_p) - \mu_v(P_v)\right] + \sigma\Omega_a$ is the energy necessary to create one cluster having a molecules

We will now manipulate this energy to prove that, provided the atmosphere is supersaturated, there exists a particular cluster size that is a boundary between energetically unfavorable growth and energetically favorable growth:

First of all, the potential of a condensed phase depends very little on pressure, so that $\mu_p(P_p) \simeq \mu_p(P_v)$ and $\Delta G \simeq a\left[\mu_p(P_v) - \mu_v(P_v)\right] + \sigma\Omega_a$

Also, the potential of the gas phase is

$$\mu_v(P_v) = \mu_v(activity = 1) + kTln\frac{P_v}{P_v^s} \qquad 5.2.10$$

As we have $\mu_v(activity = 1) = \mu_p$, we finally have:

$$\mu_p(P_p) - \mu_v(P_v) = -kTlnS \qquad 5.2.11$$

Where $S = \frac{P_v}{P_v^s}$ is the saturation ratio.

Using this for ΔG, we find:

$$\boxed{\Delta G = -akTlnS + \sigma\Omega_a} \tag{5.2.12}$$

Note that the free energy in the saturated condition ($S = 1$) is exactly $\sigma\Omega$, the price to pay to create the interface. When we are at subsaturated conditions ($S \leq 1$) both terms of this equation are positive, meaning that it is always energetically favorable to grow. When we at at supersaturated conditions ($S \geq 1$), the first term is negative, meaning that there might be a chance for ΔF to be negative and nucleation to be energetically favorable. Also note that this formula does not need to assume a spherical shape. However, we will now assume it to make some more precise calculations. In this case, $a = \frac{4}{3}\frac{\pi R_p^3}{v_A}$ and $\Omega = 4\pi R_p^2$

$$\boxed{\Delta G = -\frac{4}{3}\frac{\pi R_p^3}{v_p}k_T lnS + 4\pi R_p^2\sigma} \tag{5.2.13}$$

This is our final expression for the energy necessary to create a single cluster.

We see that if the saturation ratio is larger than 1 ($S > 1$) then, for some R_p, ΔG admits a maximum. If a cluster goes beyond this maximum, it then won't be able to shrink anymore because losing a molecule would then be energetically bad. This maximum gives what is called the critical cluster and the critical radius.

Putting the derivative of ΔG with respect to R_p equal to zero, we find the critical radius:

$$\boxed{R_p^* = \frac{2\sigma v_p}{kTln(S)}} \tag{5.2.14}$$

• This is exactly the Kelvin equation we found in the previous section and we see that the critical size radius is the radius R_p^* at which the saturation pressure over the droplet P_{sat,R_p^*} is equal to the partial pressure of the gas A.

Injecting this expression in the formula giving ΔG gives:

$$\boxed{\Delta G^* = \frac{4}{3}\pi\sigma R_p^{*2}} \tag{5.2.15}$$

This is the energy necessary to create a critical radius. The star is used to mark that the value is for the critical cluster.

5.2.2 Heteromolecular nucleation

Modified Gibbs-Duhem equation

Let us consider a fluid or solid chemical system with k chemical species. Let us call n_i the number of moles of the species i in the system.

Surface tension theory tells us that a fluid or a solid with a free interface has an additional internal energy term U_{inter} given by:

$$U_{inter} = \sigma\Omega \tag{5.2.16}$$

where σ is called the surface tension and Ω is the surface of the interface.

Surface tension theory also tell us that the variation of this energy during an infinitesimal evolution is given by:

$$\delta U_{inter} = \sigma d\Omega \tag{5.2.17}$$

(and not $\Omega d\sigma$ or $\sigma d\Omega + \Omega d\sigma$)

The overall internal energy differential of the chemical system is then:

$$dU = TdS - pdV + \sigma d\Omega + \sum_{i=1}^{k} \mu_i dn_i \tag{5.2.18}$$

Where μ_i is the chemical potential of the species i

The overall internal energy is:

$$U = TS - pV + \sigma\Omega + \sum_{i=1}^{k} \mu_i n_i \tag{5.2.19}$$

By differentiating this equation and comparing to the previous equation we get a Gibbs-Duhem relation for a system with an interface:

$$\boxed{SdT - Vdp + \Omega d\sigma + \sum_{i=1}^{k} n_i d\mu_i = 0} \tag{5.2.20}$$

Statistical description of the system

Let us consider two species A and B. The derivation of the formulas is similar to the homomolecular case.

Let us call $N_{a,b}$ the number of clusters composed of a molecules of A and b molecules of B. The Gibbs free energy of a cluster can be assumed to be:

$$G_{a,b} = N_{a,b}\left[a\mu_{p_A} + b\mu_{p_B} + \sigma\Omega_{a,b} + kTln\frac{N_{a,b}}{N_{tot}}\right] \quad 5.2.21$$

This being the free energy of the clusters of size (a, b) the total free energy of the system is:

$$G = \sum_{(a,b)\geq 1} N_{a,b}G_{a,b} \quad 5.2.22$$

$$G = N_{1,0}\mu_{v_A} + N_{0,1}\mu_{v_B} + \sum_{(a,b)\geq 2} N_{a,b}\left[a\mu_{p_A} + b\mu_{p_B} + \sigma\Omega_{a,b} + kTln\frac{N_{a,b}}{N_{tot}}\right] \quad 5.2.23$$

5.2.24

Energetics of the cluster

The derivation of the free energy necessary to create one cluster is straightforward. We have to solve $\delta G_{T,P} = 0$ with the two constraints of conservation of the number of A and B molecules. Fllowing a similar path as with the derivation in the homomolecular case the result is:

$$N_{a,b} = N_{tot}e^{-\frac{\Delta G(a,b)}{kT}} \quad 5.2.25$$

with

$$\Delta G(a,b) = a\left[\mu_{p_A}(P_p) - \mu_{v_A}(P_v)\right] \quad 5.2.26$$

$$+b\left[\mu_{p_B}(P_p) - \mu_{v_B}(P_v)\right] + 4\pi\sigma R_p^2 \quad 5.2.27$$

As in the previous case, we are going to arrange this expression to show that there is a favored cluster.

Let us first arrange $\Delta\mu_A = \mu_{p_A}(P_p) - \mu_{v_A}(P_v)$:

There is little error in replacing P_p by P_v as the condensed phase' potential varies little with pressure: $\Delta\mu_A = \mu_{p_A}(P_v) - \mu_{v_A}(P_v)$

When we write $\mu_{p_A}(P_v)$ we must account for the dependence of the free energy with the activity which is not 1 as in the homomolecular case, indeed:

$$\mu_{p_A}(P_v) \;= \mu_{p_A}(activity) \;= \mu_{p_A}(activity = 1) + kTlnAct_A \tag{5.2.28}$$

Act_A is the activity of A is the liquid phase

The same kind of relation holds for the vapor phase:

$$\mu_{v_A}(P_v) \;= \mu_{v_A}(activity) \;= \mu_{v_A}(activity = 1) + kTln\frac{P_A}{P_A^s} \tag{5.2.29}$$

P_A is the partial pressure of A. P_A^s is the saturation pressure of A

Now, when we make the difference of those last two equations, the parts of the free energy that do not depend on the activities can be treated as in the homomolecular case to give:

$$\Delta\mu_A \;=\; kTlnAct_A - kTln\frac{P_{v_A}}{P_A^s} \tag{5.2.30}$$

Finally, we have:

$$\Delta\mu_A \;=\; -kTln\frac{P_{v_A}}{Act_A p_A^s} \tag{5.2.31}$$

And $Act_A p_A^s$ is nothing else but the saturation pressure of A over a flat solution of the same composition than the cluster: $p_A^{s_{sol}}$.

$$\boxed{\Delta G(a,b) \;=\; -akTln\left(\frac{P_A}{P_A^{s_{sol}}}\right) - bkTln\left(\frac{P_B}{P_B^{s_{sol}}}\right) + 4\pi\sigma R_p^2} \tag{5.2.32}$$

We can replace R_p using:

$$av_A + bv_B = \frac{4}{3}\pi R_p^3 \tag{5.2.33}$$

Where v_A and v_B are respectively the volume occupied by a molecule of A and B in the condensed phase.

$$\Delta G(a,b) = -akTln\left(\frac{P_A}{P_A^{s_{sol}}}\right) - bkTln\left(\frac{P_B}{P_B^{s_{sol}}}\right) + 4\pi\sigma\left(\frac{3}{4\pi}(av_A + bv_B)\right)^{\frac{2}{3}} \quad 5.2.34$$

Nucleation will be able to occur if both species are supersaturated with respect to the solution (supersaturation with respect to the pure component is not necessary anymore). That is the reason why binary nucleation can have a so great importance in some systems.

The critical cluster can now be found. Its composition is given by

$$\frac{\partial \Delta G}{\partial a} = \frac{\partial \Delta G}{\partial b} = 0$$

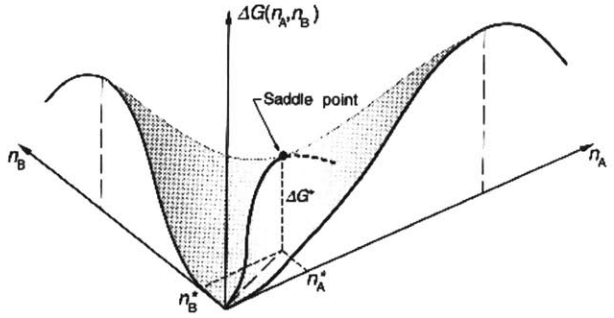

Figure 5.1: Typical free energy surface for binary nucleation. The free energy barrier is found at a saddle point which also gives the critical composition a^* b^* of the critical cluster

As in the homogeneous case the star * will indicate that the term is for the critical cluster.

We will now compute $\frac{\partial G}{\partial a}$.

For this, let's compute $dG_{P,T}$. At constant temperature and pressure, the modified Gibbs-Duhem equation that we wrote earlier in this section is: $\Omega d\sigma + \sum_i n_i d\mu_i = 0$, so that

$$\frac{\partial G}{\partial a} = -kTln\left(\frac{P_A}{P_A^{s_{sol}}}\right) + 4\pi\sigma\frac{2}{3}\frac{3v_A}{4\pi}\frac{1}{R_p} \quad 5.2.35$$

$$\frac{\partial G}{\partial a} = -kTln\left(\frac{P_A}{P_A^{s_{sol}}}\right) + \frac{2\sigma}{R_p}v_A \quad 5.2.36$$

So, the equations for the localization of the saddle point are:

$$\Delta\mu_A + \frac{2\sigma}{R_p^*}v_a = 0 \quad 5.2.37$$

$$\Delta\mu_B + \frac{2\sigma}{R_p^*}v_b = 0 \quad 5.2.38$$

Introducing $x_B = \frac{b}{a+b}$ and $v = (1-x_B)v_A + x_B v_B$ the above system is equivalent to:

$$R_p^* = \frac{-2\sigma v}{(1-x_B^*)\Delta\mu_A + x_B^*\Delta\mu_B} \quad 5.2.39$$

$$0 = v_B\Delta\mu_A - v_A\Delta\mu_B \quad 5.2.40$$

The last equation we wrote is the one which permits the location the critical nucleus

$$\boxed{\begin{array}{rl} & v_B\Delta\mu_A - v_A\Delta\mu_B = 0 \\ \Leftrightarrow & v_B ln\left(\frac{P_A}{P_A^{s_{sol}}}\right) - v_A ln\left(\frac{P_B}{P_B^{s_{sol}}}\right) = 0 \end{array}} \quad (5.2.41)$$

Once the critical (a^*, b^*) composition is found from the latter equation, we have

$$R_p^* = \frac{2\sigma v}{(1-x_B^*)kTlnS_A^* + x_B^* kTlnS_B^*} \quad 5.2.42$$

$$R_p^* = \frac{2\sigma v}{kTlnS^*} \quad 5.2.43$$

Where $S^* = S_A^{*(1-x_B^*)}S_B^{*x_B^*}$ and S_A^* S_B^* are the saturation ratios of A and B with respect to the solution.

And, after some calculations, ΔG^* is, as in homogeneous nucleation:

$$\boxed{\Delta G^* = \frac{4}{3}\pi\sigma R_p^{*2}} \quad (5.2.44)$$

5.3 Kinetics: nucleation rate

We now know the composition of the critical nucleus, we want to know the **kinetics** and how many stable nuclei are formed per unit time per unit volume.

5.3.1 Homomolecular nucleation

Let's call $f_i(t)$ the number of clusters of size i (f_i is not necessarily equal to N_i which is the equilibrium distribution)

We respectively call R_i and $\overline{R_i}$ the condensation rate and vaporisation rate of a single water molecule on a cluster of size i.

We define

$$J_{i->i+1} = R_i f_i - \overline{R_{i+1}} f_{i+1} \tag{5.3.1}$$

the net rate at which clusters of size i become clusters of size $i+1$.

The forward rate R_i

From chapter one, we know that the total number of collisions between a cluster of size i and a molecule is:

$$Z = \left(\frac{8kT}{\pi}\left(\frac{1}{m_1}+\frac{1}{m_i}\right)\right)^{\frac{1}{2}} \pi(r_1+r_i)^2 f_i f_1 \tag{5.3.2}$$

$$\iff Z = \left(\frac{8\pi kT}{m_1}\right)^{\frac{1}{2}} \left(1+\frac{1}{i}\right)^{\frac{1}{2}} r_1^2(1+i^{\frac{1}{3}})^2 f_i f_1 \tag{5.3.3}$$

$$\iff Z = \left(\frac{kT}{2\pi m_1}\right)^{\frac{1}{2}} \left(1+\frac{1}{i}\right)^{\frac{1}{2}} a_1(1+i^{\frac{1}{3}})^2 f_i f_1 \tag{5.3.4}$$

Where a_1 is the surface of a molecule.

This formula is often approximated by making 2 approximations ($(r_1+r_i)^2 \simeq r_i^2$ and $\left(\frac{1}{m_1}+\frac{1}{m_i}\right) \simeq \frac{1}{m_1}$) and simplified to:

$$Z = \left(\frac{kT}{2\pi m_1}\right)^{\frac{1}{2}} 4\pi r_i^2 f_i f_1 \tag{5.3.5}$$

$$Z = \left(\frac{P_{V,1}}{2\pi kT m_1}\right)^{\frac{1}{2}} 4\pi r_i^2 f_i \tag{5.3.6}$$

Where we used $P_{V,1} = f_1 kT$

By looking at this last formula, we see that the forward rate is:

$$\boxed{R_i = \frac{P_{V,1}}{(2\pi m_1 kT)^{\frac{1}{2}}} \Omega_i} \tag{5.3.7}$$

Where Ω_i is the surface of a cluster of size i

We also identify here $\beta_1 = \frac{P_{V,1}}{(2\pi m_1 kT)^{\frac{1}{2}}}$ which is the impinging rate of monomers (vapor molecules) (=number of collisions of monomers per unit surface)

The reverse rate $\overline{R_i}$

Let's consider an atmosphere where the population is at equilibrium, that is to say when $f_i = N_i$, the equilibrium distribution. In this case, there is no net flux of particles and $J_{i->i+1} = 0$ which yields

$$\boxed{\overline{R_{i+1}} = \frac{R_i N_i}{N_{i+1}}} \tag{5.3.8}$$

The Nucleation rate

We consider that we are in a steady state, ie $J_{i->i+1} = J$, independent of i

This gives that:

$$J = R_i f_i + \overline{R_{i+1}} f_{i+1} \tag{5.3.9}$$

$$\iff J = N_i R_i \left[\frac{f_i}{N_i} + \frac{\overline{R_{i+1}}}{N_i R_i} f_{i+1} \right] \tag{5.3.10}$$

$$\iff J = N_i R_i \left[\frac{f_i}{N_i} - \frac{f_{i+1}}{N_{i+1}} \right] \tag{5.3.11}$$

$$\iff \sum_{i=1}^{\infty} \frac{J}{N_i R_i} = \sum_{i=1}^{\infty} \left(\frac{f_i}{N_i} - \frac{f_{i+1}}{N_{i+1}} \right) \tag{5.3.12}$$

The boundary conditions for f_i are the following: $f_1 \simeq N_1$ because the monomer population is enormous enough to not have to deviate much from the equilibrium distribution to create a nucleation rate and $f_{i \gg i^*} = 0$ so that:

$$\iff \sum_{i=1}^{\infty} \frac{J}{N_i R_i} = \frac{f_1}{N_1} = 1 \tag{5.3.13}$$

5.3.14

So,

$$\boxed{J = \left(\sum_{i=1}^{\infty} \frac{1}{R_i N_i} \right)^{-1}} \tag{5.3.15}$$

This is an exact formula giving the nucleation rate. But this formula is unusable for practical purposes and the next section is dedicated to finding usuable approximations for it.

Approximation of the nucleation rate

The last formula we found in the last section is never used as it stands. This section is devoted to make an approximation of this formula.

We have:

$$J = \left(\sum_{i=1}^{\infty} \frac{1}{R_i N_i}\right)^{-1} \quad 5.3.16$$

$$N_i = N_1 e^{-\frac{\Delta G(i)}{kT}} \quad 5.3.17$$

$$\Delta G(i) = -ikTlnS + \sigma\Omega = -ikTlnS + \sigma(36\pi)^{\frac{1}{3}}(v_1 i)^{\frac{2}{3}} \quad 5.3.18$$

Calling $\theta = \frac{\sigma(36\pi)^{\frac{1}{3}}(v_1)^{\frac{2}{3}}}{kT} = \frac{\sigma\Omega}{kTi^{\frac{2}{3}}}$, we have:

$$J = N_1 \left(\sum_{i=1}^{\infty} \frac{1}{R_i e^{-\theta i^{\frac{2}{3}} + ilnS}}\right)^{-1} \quad 5.3.19$$

1) We see that the exponent in the exponential is the free energy of formation of a cluster of size i (divided by kT)

2) R_i is proportional to the surface of the cluster ($\sim i^{\frac{2}{3}}$) and has little influence on the global behavior of the denominator compared to the exponential.

3) We saw that the free energy of a cluster is a function that first grows, reaches a maximum and then decreases again.

All this leads us to say that the terms in the sum will be greatest around i^*, the number of molecules corresponding to the critical cluster.

We can make the following approximation:

$$J \simeq N_1 R_{i^*} \left(\sum_{i=1}^{\infty} \frac{1}{e^{-\theta i^{\frac{2}{3}} + ilnS}}\right)^{-1} \quad 5.3.20$$

Then, we approximate $-\theta i^{\frac{2}{3}} + ilnS$ by a Taylor development around i^*, using $R_p^* = \frac{2\sigma}{kTlnS} = \left(i^* v_p \frac{3}{4\pi}\right)^{\frac{1}{3}}$ we get:

$$-\theta i^{\frac{2}{3}} + ilnS \simeq (-\theta i^{*\frac{2}{3}} + i^* lnS) + \frac{1}{2}\frac{d^2}{di^2}\left(-\theta i^{\frac{2}{3}} + ilnS\right)|_{i=i^*} (i - i^*)^2 \quad 5.3.21$$

$$-\theta i^{\frac{2}{3}} + ilnS \simeq -\frac{\Delta G^*}{kT} + \frac{1}{9}\theta i^{*-\frac{4}{3}}(i - i^*)^2 \quad 5.3.22$$

$$-\theta i^{\frac{2}{3}} + ilnS \simeq -\frac{\Delta G^*}{kT} + \frac{1}{9}\frac{\sigma\Omega}{kTi^{*2}}(i - i^*)^2 \quad 5.3.23$$

And extending the range of integration to $[-\infty \ +\infty]$, we get:

$$\boxed{J \simeq N_1 R_{i^*} \left(\frac{\sigma\Omega}{9\pi kTi^{*2}}\right)^{\frac{1}{2}} e^{-\frac{\Delta G^*}{kT}}} \tag{5.3.24}$$

We call $Z = \left(\frac{\sigma\Omega}{9\pi kTi^{*2}}\right)^{\frac{1}{2}} = \left(\frac{\Delta G^*}{3\pi kTi^{*2}}\right)^{\frac{1}{2}} = \sqrt{\frac{\sigma}{kT}}\frac{v_p}{2\pi R_p^{*2}}$ is called the Zeldovich factor.

By replacing R_{i^*} we also get:

$$\boxed{J = 4\pi r_{i^*}^2 N_1^2 \left(\frac{kT}{2\pi m_1}\right)^{\frac{1}{2}} Z e^{-\frac{\Delta G^*}{kT}}} \tag{5.3.25}$$

$$\boxed{J = 4\pi r_{i^*}^2 N_1^2 \left(\frac{kT}{2\pi m_1}\right)^{\frac{1}{2}} \sqrt{\frac{\sigma}{kT}}\frac{v_p}{2\pi R_p^{*2}} e^{-\frac{\Delta G^*}{kT}}} \tag{5.3.26}$$

- Note that the nucleation rate is of the form $J = Ce^{-\frac{\Delta G^*}{kT}}$, showing the discrepancy between the energetical part of the nucleation rate $e^{-\frac{\Delta G^*}{kT}}$ and a mainly kinetic part C
- Note that the kinetic prefactor C can be decomposed into:

$$C = N_{tot} * \Omega_{i^*} * \beta_1 * Z \tag{5.3.27}$$

Where N_{tot} is the total number of particles (including monomers) in the system ($N_{tot} \simeq N_1$) ; Ω_{i^*} is the surface of the critical cluster ; $\beta_1 = N_1 \left(\frac{kT}{2\pi m_1}\right)^{\frac{1}{2}}$ is the impinging rate of monomers ; Z is the Zeldovich factor $Z = \sqrt{\frac{\sigma}{kT}}\frac{v_p}{2\pi R_p^{*2}}$

5.3.2 Heteromolecular nucleation

We will only deal with binary nucleation.

We will show in this part that the nucleation rate for binary nucleation can, as in the homomolecular case, be approximated by a formula of the form:

$$J = Ce^{-\frac{\Delta G^*}{kT}} \tag{5.3.28}$$

There are many different ways to compute the preexponential factor C and this has been the subject of many papers over the course of the last 50 years.

We will present here commonly accepted methods. There are several other methods. The derivation of this method will be given in an appendix.

Imagine a mixture of molecules of a gas A and molecules of a gas B

The preexponential factor is:

$$C = N_{tot}\Omega_{a^*,b^*}\beta_{AV}Z \tag{5.3.29}$$

Where:

$\rightarrow N_{tot}$

N_{tot} is the total concentration of particles (including monomers) in the system.

$\rightarrow \Omega_{a^*,b^*}$

Ω_{a^*,b^*} is the surface of the critical nucleus

$\rightarrow \beta_{AV}$

There are 2 main ways to compute β_{AV}

• There are "more precise" descriptions of the impinging rates which lead to the following formula:

$$\beta_{AV} = \frac{\beta_{AA}\beta_{BB} - \beta_{AB}^2}{\beta_{AA}sin^2\phi + \beta_{BB}cos^2\phi - 2\beta_{AB}sin\phi cos\phi} \tag{5.3.30}$$

Where:

$$\beta_{AA} = \sum_{(a,b)<(a^*,b^*)} a^2\beta_{a,b} \tag{5.3.31}$$

$$\beta_{BB} = \sum_{(a,b)<(a^*,b^*)} b^2\beta_{a,b} \tag{5.3.32}$$

$$\beta_{AB} = \sum_{(a,b)<(a^*,b^*)} ab\beta_{a,b} \tag{5.3.33}$$

5.3.34

The $\beta_{a,b}$ are the impinging rates on the critical cluster of clusters of size (a,b).

ϕ is the angle beetween the b-axis and the direction of growth of the critical cluster on a (a, b) diagram.

• In systems where the species B is less abundant than the species A (like sulfuric acid in the sulfuric acid-water mixture), we can say that is it the impinging rate of the less abundant species which limits the nucleation and take β_{AV} as the impinging rate of this species.

$$\beta_{AV} = N_b \left(\frac{kT}{2\pi m_b} \right)^{\frac{1}{2}} \quad 5.3.35$$

$\rightarrow Z$

There are 2 main ways to compute Z:

• The more precise description:

$$Z = -\frac{D^r}{(-detD)^{\frac{1}{2}}} \quad 5.3.36$$

Where $D^r = D_{aa}cos^2\phi + D_{bb}sin^2\phi + 2D_{ab}cos\phi sin\phi$ and $detD = D_{aa}D_{bb} - D_{ab}D_{ab}$ and $D_{ij} = \frac{\partial \Delta G}{\partial i \partial j}$

• The simplified description:

The idea of the simplified description is to imagine that there exists a "virtual monomer" having the composition of the critical cluster and that this monomer nucleates. This way, the Zeldovich factor is the same as in the homomolecular case:

$$Z = \sqrt{\frac{\sigma}{kT}} \frac{v_{virt}}{2\pi R_p^{*2}} \quad 5.3.37$$

$v_{virt} = (1 - x_B^*)v_A^* + x_B^* v_B^*$ is the volume of the virtual monomer

$\rightarrow \phi$

There are 3 main ways to compute ϕ:

• The more precise description:

ϕ is obtained by resolving the following (but never used in practice) equation:

calling $R_{ij} = \beta_{ij} * \Omega_{a^*,b^*}$

$$tan^4\phi \left[D_{bb}R_{AA}R_{AB} + D_{ab}R_{AA}^2\right] + \quad 5.3.38$$

$$tan^3\phi \left[D_{aa}R_{AA}^2 - D_{bb}R_{AA}R_{BB} - 2D_{bb}R_{AB}^2 - 2D_{ab}R_{AA}R_{AB}\right] + \quad 5.3.39$$

$$tan^2\phi \left[-3D_{aa}R_{AA}R_{AB} + 3D_{bb}R_{BB}R_{AB}\right] + \quad 5.3.40$$

$$tan\phi \left[2D_{aa}R_{AB}^2 + D_{aa}R_{AA}R_{BB} - D_{bb}R_{BB}^2 + 2D_{ab}R_{BB}R_{AB}\right] + \quad 5.3.41$$

$$\left[-D_{aa}R_{BB}R_{AB} - D_{ab}R_{BB}^2\right] = 0 \quad 5.3.42$$

• A simplified description:

The above equation can be simplified in many cases, especially in systems where a species is less abundant than the other (like sulfuric acid in the sulfuric acid-water mixture). In this case the direction of growth of the cluster is given by:

$$tan\phi = -\frac{D_{aa}}{D_{ab}} \quad 5.3.43$$

• Another simplified approximation:

Another approximation consists in saying that the angle of growth is given by:

$$tan\phi = \frac{b^*}{a^*} \quad 5.3.44$$

Choice

Any combination of the above possibilities can be adopted (all combinations have been used for practical applications). For a comparison of different choices see [21]

Chapter 6

The $H_2O - H_2SO_4$ System

The work in this chapter is based on [36],[43],[18],[47],[55],[33],[34][53],[54],[21],[48].

The $H_2O - H_2SO_4$ system is a system of special interest for us as it plays a key role in particle formation as soon as sulfur VI is available. This chapter is devoted to applying the results of the previous chapter to the particular case of the $H_2O - H_2SO_4$ mixture. The first section of this chapter will be devoted to the determination of the energetics of the critical nucleus: ΔG^*, a^*, b^*, R_p^*. The second section of this chapter will be devoted to the determination of the nucleation rate.

In the rest of this chapter the gas A will be water, and the gas B will be the sulfuric acid.

6.1 Energetics

We saw in the last chapter that the localization of the saddle point was obtained by finding a composition (a, b) for a cluster which obeys:

$$\boxed{\begin{aligned} & v_B\Delta\mu_A - v_A\Delta\mu_B && = 0 \\ \Leftrightarrow \quad & v_B ln\left(\frac{P_A}{P_A^{sol}}\right) - v_A ln\left(\frac{P_B}{P_B^{sol}}\right) && = 0 \\ \Leftrightarrow \quad & v_B ln\left(\frac{\frac{P_A}{P_A^{sol}}}{Act_A}\right) - v_A ln\left(\frac{\frac{P_B}{P_B^{sol}}}{Act_B}\right) && = 0 \end{aligned}} \tag{6.1.1}$$

P_A and P_B are given: They are the partial pressure of gaseous water and the partial

pressure of gaseous sulfuric acid in the mixture.

We need to be able to determine:

- P_A^s, P_B^s, the saturation pressures of water and sulfuric acid
- Act_A and Act_B which are respectively the activity of water in a solution of acid sulfuric and the activity of sulfuric acid in a solution of sulfuric acid.

Saturation pressures

We use interpolation formulas ([53], [54]):

(T in Kelvin, Pressures in Pascals)

$$P_A^s = exp\left(77.34491296 - \frac{7235.424651}{T} - 8.2ln(T) + 5.7113E-3T\right) \quad 6.1.2$$

$$P_B^s = 101325exp\left(-11.695 + 10156\left[\frac{1}{360.15} - \frac{1}{T} + \frac{0.38}{545} * \left(1 + ln\left(\frac{360.15}{T} - \frac{360.15}{T}\right)\right)\right]\right) \quad 6.1.3$$

Activities in the liquid phase

The activities in the liquid phase are obtained by using the interpolation curves from [48]:

For of mole fraction of water of X_1 and of acid of X_2 at a temperature T:

$$Act_{water} = \frac{X_1}{X_1 + X_2} * 10^{\frac{A1(T)}{T}\frac{X_2^2}{(X_2 + B1 * X_1)^2}} \quad 6.1.4$$

where $B1 = 0.527$, and $A1(T) = 2.989 * 10^3 - \frac{2.147*10^6}{T} + \frac{2.33*10^8}{T^2}$

$$Act_{acid} = \frac{X_2}{X_1 + X_2} * 10^{\frac{A2(T)}{T}\frac{X_1^2}{(X_1 + B2 * X_1)^2}} \quad 6.1.5$$

where $B2 = 1/0.527$, and $A2(T) = 5.672 * 10^3 - \frac{4.074*10^6}{T} + \frac{4.421*10^8}{T^2}$

Saddle point

With the information that we now have, we can determine the location of the saddle point a^*, b^* and ΔG^*

However, the $H_2O - H_2SO_4$ mixture has a peculiarity that will be presented in the next subsection

6.1.1 Effect of Hydrates

A peculiarity of the $H_2O - H_2SO_4$ mixture is the tendency of H_2SO_4 molecules to be hydrated (they are then called hydrates) even prior to the nucleation. This has a twofold effect: First, hydrates reduce the amount of available H_2SO_4 molecules, hence they reduce the energetical appeal to nucleate and reduce the energetical factor of the nucleation rate. Second, when hydrates collide with a cluster, they bring several molecules at once, hence they increase the kinetic prefactor of the nucleation rate.

This subsection is devoted to present the effect of hydrates on the energetical part of the nucleation rate.

To evaluate this effect we need to make a complete chemical description of the system.

Call $N(h,1)$ the number of hydrates (per unit volume) containing h molecules of water.

Call N_1 and N_2 the *total* number of water and acid molecules (per unit volume).

Call $\overline{N}_1$ and $\overline{N}_2$ the number of remaining free water and acid molecules (per unit volume).

We have the relations:

$$N_1 = \overline{N}_1 + \sum_h hN(h,1) \tag{6.1.6}$$

$$N_2 = \overline{N}_2 + \sum_h N(h,1) \tag{6.1.7}$$

Effect on saddle point localization

In the equation for the saddle point localization

$$v_B ln\left(\frac{\frac{P_A}{P_A^s}}{Act_A}\right) - v_A ln\left(\frac{\frac{P_B}{P_B^s}}{Act_B}\right) = 0 \tag{6.1.8}$$

P_B is the partial pressure of only the *free* H_2SO_4 molecules. Hence, the presence of hydrates changes the localization of the saddle point.

Effect on energy

If we denote $\overline{\Delta G}(h,1)$ as the free energy necessary to create and hydrate $(h,1)$, the number of such hydrates will be:

$$N(h,1) = N_t e^{-\frac{\overline{\Delta G}(h,1)}{kT}} \quad 6.1.9$$

Where N_t is the total number of particles all of types (including hydrates). In practice, we are interested in situations where the number of water molecules far exceeds the number of sulfuric acid molecules and in this case: $N_t \simeq N_1 \simeq \overline{N}_1$.

In conventional nucleation theory, hydrates are treated as liquid drops and their free energy of formation is:

$$\overline{\Delta G}(h,1) = h\left[\overline{\mu}_{l1} - \overline{\mu}_{v1}\right] + \left[\overline{\mu}_{l2} - \overline{\mu}_{v2}\right] + \sigma(h,1)\Omega(h,1) \quad 6.1.10$$

The subscripts 1 and 2 respectively refer to water and acid molecules. The subscripts v and l respectively refer to the vapor and the liquid. $\Omega(h,1)$ is the surface area of the hydrate. (When we overline a quantity, it means that it takes the hydrates into consideration).

$\overline{\mu}_{v1}$ and $\overline{\mu}_{v2}$, the chemical potentials of water and acid molecules in an atmosphere containing hydrates are quantities that are difficult to evaluate. What is easier to compute are the same values in an atmosphere without hydrates. This is why we will express $\overline{\Delta G}(h,1)$ as a function of $\Delta G(h,1)$, the free energy of creation of an hydrate calculated as though all molecule of water (N_1) and acid (N_2) are free. There is an simple relation between $\overline{\Delta G}(h,1)$ and $\Delta G(h,1)$:

$$\overline{\Delta G}(h,1) = \Delta G(h,1) + kTln\frac{N_2}{\overline{N}_2} + hkTln\frac{N_1}{\overline{N}_1} \quad 6.1.11$$

and, using $N_t \simeq N_1 \simeq \overline{N}_1$, we obtain:

$$N(h,1) = N_1\left(\frac{\overline{N}_2}{N_2}\right)e^{-\frac{\Delta G(h,1)}{kT}} \quad 6.1.12$$

$\overline{\Delta G^*}$ is the free energy necessary to form a critical nucleus.

$$\overline{\Delta G^*} = \overline{n^*}_1 \left[\overline{\mu}_{l1} - \overline{\mu}_{v1}\right] + \overline{n^*}_2 \left[\overline{\mu}_{l2} - \overline{\mu}_{v2}\right] + \sum n_h^* \left[\mu_{lh} - \mu_{vh}\right] + \sigma\Omega \qquad 6.1.13$$

n_h indicates the number of hydrates (1,h) incorporated into the droplet.

As said before, this free energy contains terms that are difficult to evaluate because the vapor phase (principally the acid) is perturbed by the presence of hydrates. This is the reason we will now relate the free energy $\overline{\Delta G}$ where hydrates are taken into account to the free energy ΔG calculated as if all water and acid molecules were free.

As seen, ΔG is equal to

$$\Delta G = n_1 ln \left[\mu_{l1} - \mu_{v1}\right] + n_2 \left[\mu_{l1} - \mu_{v1}\right] + \sigma\Omega \qquad 6.1.14$$

$$\Delta G = -n_1 kTln\left(\frac{p_1}{p_1^{s_{sol}}}\right) - n_2 kT\left(\frac{p_2}{p_2^{s_{sol}}}\right) + \sigma\Omega \qquad 6.1.15$$

Where $p_1^{s_{sol}}$ and $p_2^{s_{sol}}$ are respectively the saturation pressure of water and sulfuric acid above a (flat) solution of the same composition of the droplet.

Now if we include the hydrates, this free energy becomes:

$$\overline{\Delta G} = \overline{n}_1 ln \left[\overline{\mu}_{l1} - \overline{\mu}_{v1}\right] + \overline{n}_2 \left[\overline{\mu}_{l2} - \overline{\mu}_{v2}\right] + \sum n_h \left[\mu_{lh} - \mu_{vh}\right] + \sigma\Omega \qquad 6.1.16$$

Since there is "chemical" equilibrium between the hydrates and the free molecules, we have:

$$\mu_{lh} = h\overline{\mu}_{l1} + \overline{\mu}_{l2} \qquad 6.1.17$$

$$\mu_{vh} = h\overline{\mu}_{v1} + \overline{\mu}_{v2} \qquad 6.1.18$$

So our last formula becomes:

$$\overline{\Delta G} = (\overline{n}_1 + \sum hn_h)\left[\overline{\mu}_{l1} - \overline{\mu}_{v1}\right] + (\overline{n}_2 + \sum n_h)\left[\overline{\mu}_{l2} - \overline{\mu}_{v2}\right] + \sigma\Omega \qquad 6.1.19$$

$$\Longleftrightarrow \overline{\Delta G} = n_1 \left[\overline{\mu}_{l1} - \overline{\mu}_{v1}\right] + n_2 \left[\overline{\mu}_{l2} - \overline{\mu}_{v2}\right] + \sigma\Omega \qquad 6.1.20$$

$$\Longleftrightarrow \overline{\Delta G} = -n_1 kTln\left(\frac{\overline{p}_1}{\overline{p}_1^{s_{sol}}}\right) - n_2 kTln\left(\frac{\overline{p}_1}{\overline{p}_1^{s_{sol}}}\right) + \sigma\Omega \qquad 6.1.21$$

It can be compared to the free energy without hydrates. The difference is:

$$\overline{\Delta G} - \Delta G = n_2 kT ln\left(\frac{p_2 \overline{p}_2^{s_{sol}}}{\overline{p}_2 p_2^{s_{sol}}}\right) \quad 6.1.22$$

(we used the fact that the water is little perturbed by the hydrates ($\overline{p}_1^{s_{sol}} \simeq p_1^{s_{sol}}$ $\overline{p}_1 \simeq p_1$)

Computation of the hydrates distribution

We need to have the distribution of hydrates to the evaluate $\frac{p_2 \overline{p}_2^{s_{sol}}}{\overline{p}_2 p_2^{s_{sol}}}$.

Let us consider the following reactions:

$$\overline{N}_1 + \overline{N}_2 \rightleftharpoons N(1,1)$$
$$\overline{N}_1 + N(1,1) \rightleftharpoons N(1,2)$$
$$\vdots$$
$$\overline{N}_1 + N(1,h-1) \rightleftharpoons N(1,h)$$

Calling N_0 the overall number density of the gas phase, the law of mass action gives:

$$K_1 = \frac{\frac{N(1,1)}{N_0}}{\frac{\overline{N}_1}{N_0}\frac{\overline{N}_2}{N_0}} = \frac{N(1,1)N_0}{\overline{N}_1 \overline{N}_2} \quad 6.1.23$$

$$K_2 = \frac{N(1,2)N_0}{\overline{N}_1 N(1,1)} = \frac{N(1,2)N_0^2}{\overline{N}_1^2 \overline{N}_2 K_1} \quad 6.1.24$$

$$\vdots$$

$$K_h = \frac{N(1,h)N_0}{\overline{N}_1 N(1,h-1)} = \frac{N(1,h)N_0^h}{\overline{N}_1^h \overline{N}_2 K_1 K_2 \cdots K_{h-1}} \quad 6.1.25$$

Finally, by using $\sum N(1,h) = N_2$, we get the number density of free acid molecules:

$$\overline{N}_2 = \frac{N_2}{1 + K_1\left(\frac{N_1}{N_0}\right) + K_1 K_2 \left(\frac{N_1}{N_0}\right)^2 + \cdots + K_1 K_2 .... K_h \left(\frac{N_1}{N_0}\right)^h} \quad 6.1.26$$

We omitted the bar over N_1 as $\overline{N}_1 \simeq N_1$.

We have the same result at saturation pressure

$$\overline{N}_2^{s_{sol}} = \frac{N_2^{s_{sol}}}{1 + K_1\left(\frac{N_1^{s_{sol}}}{N_0}\right) + K_1K_2\left(\frac{N_1^{s_{sol}}}{N_0}\right)^2 + \cdots + K_1K_2....K_h\left(\frac{N_1^{s_{sol}}}{N_0}\right)^h} \quad 6.1.27$$

Finally,

$$\overline{\Delta G} - \Delta G = n_2 kTln\left[\frac{1 + K_1\left(\frac{N_1}{N_0}\right) + K_1K_2\left(\frac{N_1}{N_0}\right)^2 + \cdots + K_1K_2....K_h\left(\frac{N_1}{N_0}\right)^h}{1 + K_1\left(\frac{N_1^{s_{sol}}}{N_0}\right) + K_1K_2\left(\frac{N_1^{s_{sol}}}{N_0}\right)^2 + \cdots + K_1K_2....K_h\left(\frac{N_1^{s_{sol}}}{N_0}\right)^h}\right] \quad 6.1.28$$

$$e^{-\frac{\overline{\Delta G}}{kT}} = \left[\frac{1 + K_1\left(\frac{N_1}{N_0}\right) + K_1K_2\left(\frac{N_1}{N_0}\right)^2 + \cdots + K_1K_2....K_h\left(\frac{N_1}{N_0}\right)^h}{1 + K_1\left(\frac{N_1^{s_{sol}}}{N_0}\right) + K_1K_2\left(\frac{N_1^{s_{sol}}}{N_0}\right)^2 + \cdots + K_1K_2....K_h\left(\frac{N_1^{s_{sol}}}{N_0}\right)^h}\right]^{n_2} \quad 6.1.29$$

We need the constants K_h.

The free energy change $\Delta^0 G_h$ for the addition of a water molecule on a cluster containing $h-1$ water molecules can be obtained by taking the derivative of $\Delta G(a,1)$ with respect to a at point $h-1$.

K_h is then given by:

$$\Delta^0 G_h = -RTlnK_h \quad 6.1.30$$

Detailed calculations of those constants are available in

We present the final results [34]:

$$K_1 = exp(\frac{6136}{T} - 14.336) \quad 6.1.31$$

$$K_2 = exp(\frac{5810}{T} - 15.51) \quad 6.1.32$$

$$K_3 = exp(\frac{4430}{T} - 12.14) \quad 6.1.33$$

$$K_4 = exp(\frac{4383}{T} - 12.60) \quad 6.1.34$$

$$K_5 = exp(\frac{4371}{T} - 12.87) \quad 6.1.35$$

6.2 Kinetics

The nucleation rate is of the form:

$$J = Ce^{-\frac{\Delta G}{kT}} \tag{6.2.1}$$

According to the last chapter, we can make the following choice for the kinetic prefactor:

$$C = 4\pi R_p^{*2} N_1 \beta_{AV} \sqrt{\frac{\sigma}{kT}} \frac{v_{virt}}{2\pi R_p^{*2}} \tag{6.2.2}$$

with

$$\beta_{AV} = \frac{\beta_1(\beta_2 + \sum_{h=1,n} \beta_{h,1}) - \left(\sum_{h=1,n} h\beta_{h,1}\right)^2}{\beta_1 sin^2\phi + (\beta_2 + \sum_{h=1,n} \beta_{h,1})cos^2\phi - 2\left(\sum_{h=1,n} h\beta_{h,1}\right) sin\phi cos\phi} \tag{6.2.3}$$

This choice for the kinetic prefactor has been found to be in reasonable agreement with experimental data [55].

$$\beta_1 = N_1 \sqrt{\frac{kT}{2\pi}\left(\frac{1}{m_1} + \frac{1}{m^*}\right)} \tag{6.2.4}$$

$$\beta_2 = \overline{N_2} \sqrt{\frac{kT}{2\pi}\left(\frac{1}{m_1} + \frac{1}{m^*}\right)} \tag{6.2.5}$$

$$\beta_{h,1} = N_h \sqrt{\frac{kT}{2\pi}\left(\frac{1}{m_h} + \frac{1}{m^*}\right)} \tag{6.2.6}$$

n is the number of hydrate that we take into account. We will never go above $n = 5$ as those hydrates are extremely rare at the water partial pressures commonly found in aeronautical applications

Chapter 7

Plume and Probe Modeling

In an effort to characterize particulate matter production by aircraft engines, NASA directed a program called APEX (http://www.nasa.gov/centers/glenn/projects/APEX.html) in which MIT and Aerodyne Research Inc. Billerica Mass, along with other research institutions (NASA Glenn Research Center, Cleveland; NASA Langley Research Center, Hampton, Va.; NASA Dryden Flight Research Center, Edwards, Calif.; General Electric Aircraft Engines, Evendale, Ohio; The Boeing Company, Seattle, Wash.; Southwest Research Institute, San Antonio, Texas; Arnold Engineering Development Center, Arnold AFB, Tenn.; University of Missouri, Rolla, Mo.; EPA, Research Triangle Park, N.C.; Wright Patterson Air Force Base, Dayton, Ohio; University of California, Riverside, Calif.; and Process Metrics, Inc., San Ramon, Calif.) where involved.

Probes were installed at different locations behind a CFM56 aircraft engine (1m, 10m, 30m) and exhaust gas samples were taken at different power settings. The exhaust gases were then transmitted via the probes to a sampling line and finally to the analyzing instruments.

The objectives of the work in this chapter are:

- To assess the modeling methods described in Chapters 5 and 6 through comparison to the experimental data obtained in these tests. We want to determine the extent to which our modeling is able to replicate the experimental data obtained
- To explain the results obtained in the experiment by quantifying the effect of the probe and sampling line on the exhaust gas sample and determine if there is a significant evolution of the chemical and microphysical properties of the sample between the time it enters the probe and the time it reaches the analyzing instruments.

7.1 Presentation of the measurements

7.1.1 Hard and volatile contents

The following graphs are taken from a presentation at the APEX November 2004 meeting. They show the measured emission indexes of non-volatile (soot) and volatile content (sulfate and organics) at 1m and 30m for two different types of fuel (the low sulfur content is $0.38 g/kg_{fuel}$, the high sulfur content is $1.595 g/kg_{fuel}$).

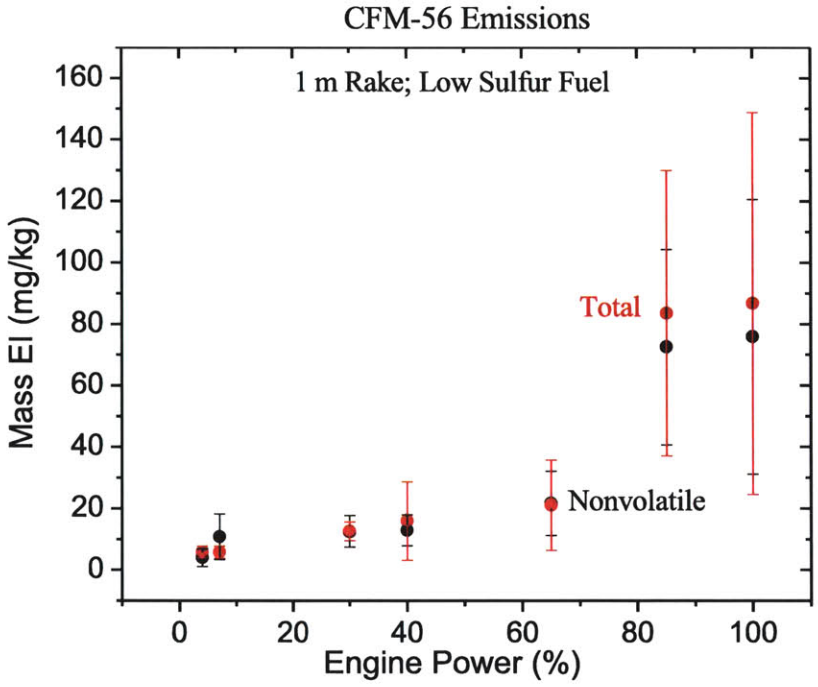

Figure 7.1: Measured emission indexes at 1m behind CFM56 engine using low sulfur fuel

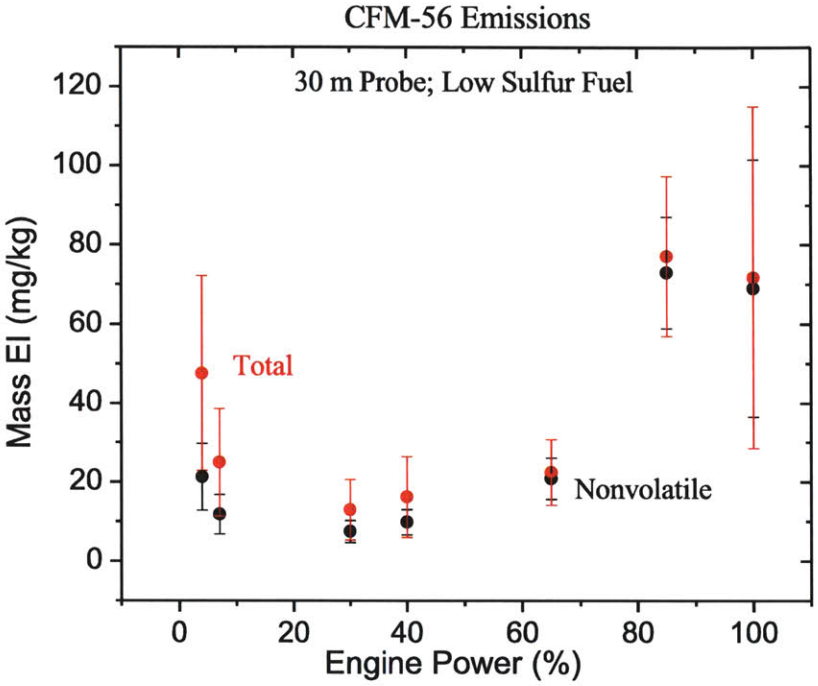

Figure 7.2: Measured emission indexes at 30m behind CFM56 engine using low sulfur fuel

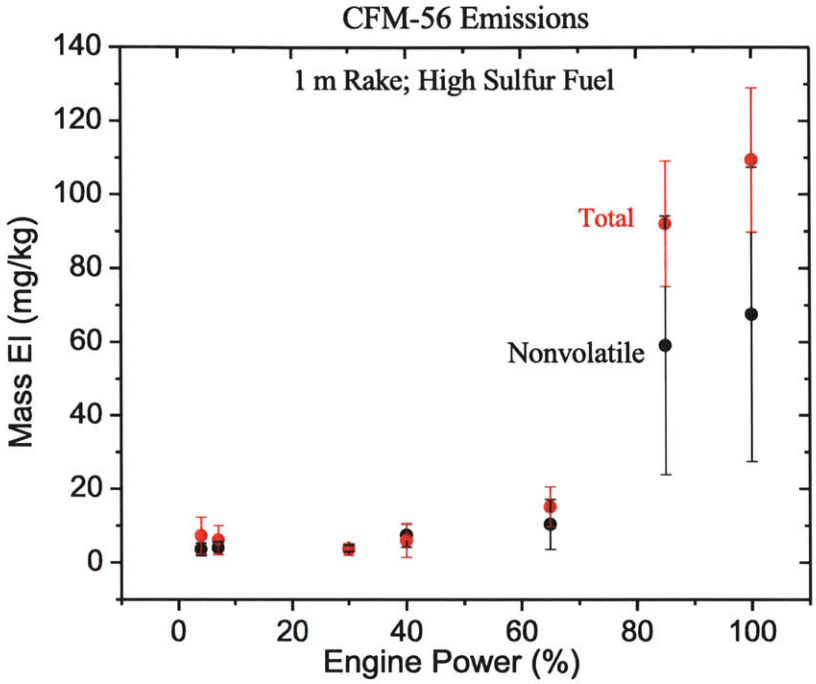

Figure 7.3: Measured emission indexes at 1m behind CFM56 engine using high sulfur fuel

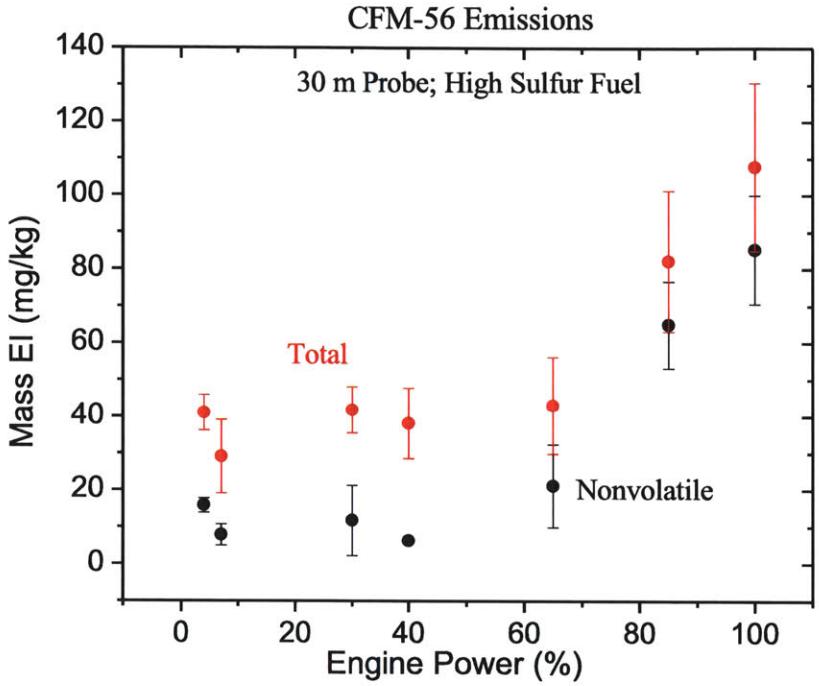

Figure 7.4: Measured emission indexes at 30m behind CFM56 engine using low sulfur fuel

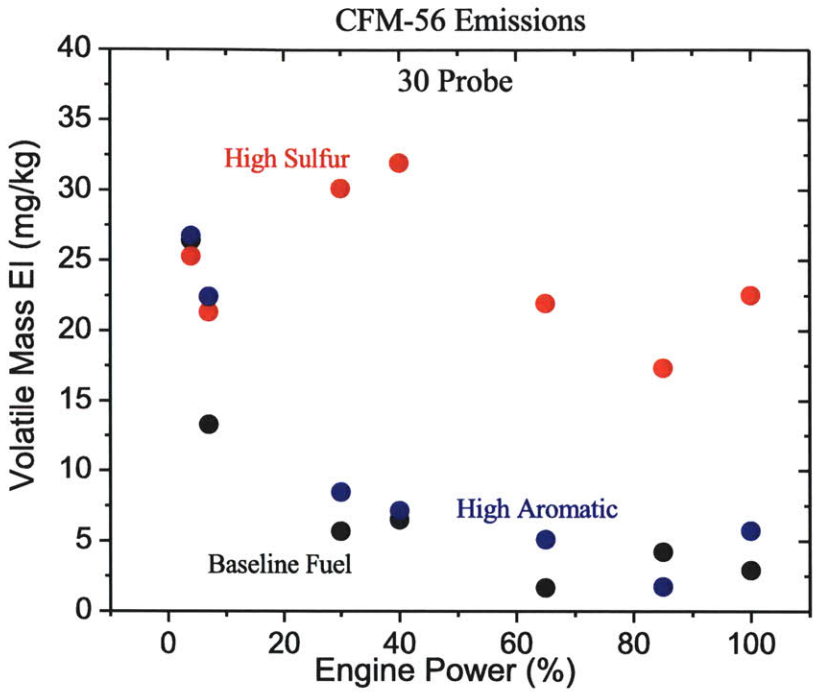

Figure 7.5: Measured volatile emission index at 30m behind CFM56 engine for 3 types of fuel including low and high sulfur content

7.1.2 Sulfate on soot

These tables present the part of the volatile content that is measured as sulfate on the soot particles. These can be put in context relative to the total fuel sulfur emissions which, for example at take off, were above $5mg/kg_{fuel}$ for the low sulfur fuel and above $20mg/kg_{fuel}$ for the high sulfur fuel.

Low sulfur content

Power (%)	Sulfate (1m) (mg/kg_{fuel})	Sulfate (10m) (mg/kg_{fuel})	Sulfate (30m) (mg/kg_{fuel})
idle	-0.0045	0.3740	1.08
65	-0.0373	0.1523 (@40%)	0.68 (@40%)
to	-0.009	0.14	1.24

High sulfur content

Power (%)	Sulfate (1m) (mg/kg_{fuel})	Sulfate (10m) (mg/kg_{fuel})	Sulfate (30m) (mg/kg_{fuel})
idle	0.0076	0.2746	0.5
65	0.0076	0.1796	1.576 (@60%)
to	0.0629	0.4316	3.28

7.2 Thermodynamical modeling of the plume

In chapter 4, we described the non-volatile PM microphysics inside the engine and came to the conclusion that once the non-volatile PM leaves the primary zone of the combustor, the thermodynamic environment inside the engine does not allow for substantial changes in the PM microphysical properties before the PM reaches the end of the engine. However, some key gas phase chemistry occures inside the engine and particularly sulfur VI creation. We used the same methods as in [22] to compute the gas phase composition and the aerosol precursor concentrations at the engine exit to use them as an input for the subsequent modeling of PM evolution in the plume. The fluid dynamic and thermodynamic conditions within the engine were estimated using detailed engine data provided by General Electric Aircraft Engines.

To model this evolution we need the thermodynamic environment to which the PM and PM precursors will be exposed, this is the purpose of this section.

We are interested in the mixing profile from a small volume of core flow leaving the engine. We model the mixing of the core flow into the bypass flow as the mixing of a core jet mixing into an infinite surrounding coflowing jet. We model the mixing of the complete exhaust flow with the rest of the atmosphere as the mixing of a jet mixing into a fluid at rest

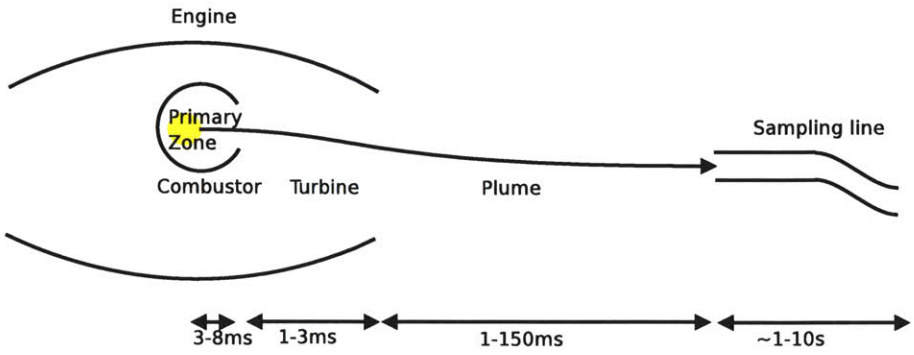

Figure 7.6: Typical flow residence times in different parts of the engine/plume/sampling-system environment

7.3 Mixing with bypass flow: Coflowing jet

The aim is to model the mixing of the core flow with the bypass flow.

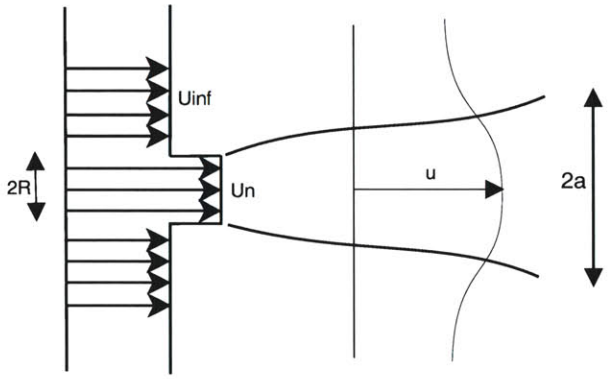

Figure 7.7: Coflowing jet

7.3.1 Centerline

We note $\Delta\overline{u}_m(x)$ the speed **excess** at the centerline at position x. $\overline{u}(x,r)$ is the speed at postion x and r. U_∞ is the external speed

According to [32]

$$\boxed{\frac{\Delta\overline{u}_m(x)}{U_\infty} = C\left(A_1 + \left(\frac{x}{\theta}\right)^2\right)^{\frac{1}{6}} \cdot \frac{\theta}{x}} \tag{7.3.1}$$

Where θ is a typical distance of the problem defined by $\theta^2 = \int_0^\infty \frac{\overline{u}}{U_\infty}(\frac{\overline{u}}{U_\infty} - 1)2\pi r dr$
The constants C and A_1 are experimentally obtained: $C \simeq 2.67$, $A_1 \simeq 299$

7.3.2 Rest of the core flow

At sufficiently large x ($x \gg R$), it becomes possible to write

$$\overline{u}(x,r) - U_\infty = \Delta\overline{u}_m(x)e^{-\frac{r^2}{a(x)^2}} \tag{7.3.2}$$

a is a dummy variable representing the "radius" of the coflowing jet, sufficiently far away from the nozzle ($x \gg R$ and $\Delta\overline{u}_m \ll (U_n - U_\infty)$)
A power law is also available for a

$$\boxed{a(x) = \frac{1}{\sqrt{C\pi}}(\theta^2 x)^{\frac{1}{3}}} \tag{7.3.3}$$

7.3.3 Species and temperature mixing

The temperature and species mixing are linked to the momentum mixing through the Prandtl number which in the case of an axisymmetric jet is $\frac{3}{4}$

$$\frac{\overline{T}(x,r) - T_\infty}{\Delta T_m(x)} = \frac{\overline{C}(x,r)}{C_m(x)} = \left(\frac{\overline{u}(x,r) - U_\infty}{\Delta u_m(x)}\right)^{\frac{3}{4}} \tag{7.3.4}$$

By writing the conservation of a species between location $x = 0$ where it has a concentration C_0 and x we get:

$$\int_{r=0}^{R_0} C_0 2\pi r dr = \int_{r=0}^{\infty} \overline{C} 2\pi r dr \tag{7.3.5}$$

$$\Leftrightarrow \quad C_0 R_0^2 = C_m(x)\frac{4\pi a(x)^2}{3} \tag{7.3.6}$$

$$\Leftrightarrow \quad \frac{C_m(x)}{C_0} = \frac{3R_0^2 C}{4(\theta^2 x)^{\frac{2}{3}}} \tag{7.3.7}$$

7.4 Mixing with atmosphere: Single Axisymmetric jet

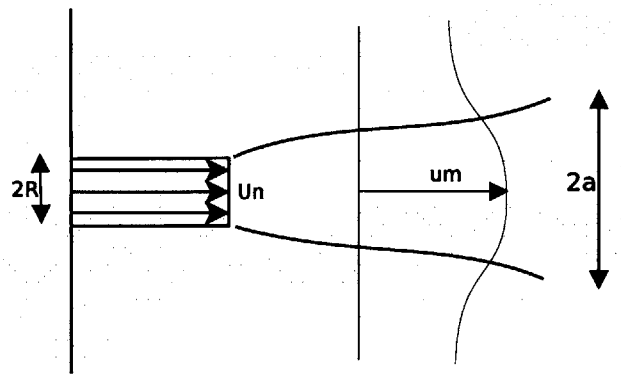

Figure 7.8: Coflowing jet

7.4.1 Centerline

We define $\overline{u}_m(x)$ as the speed at the centerline.
We call $J = \int_0^\infty \overline{u}(0,r)^2 2\pi r dr$ the momentum flux.
According to [38], we get the following power law for $\overline{u}_m(x)$:

$$\boxed{\overline{u}_m(x) = 7.32\sqrt{J}\frac{1}{x}} \tag{7.4.1}$$

7.4.2 Rest of the core flow

We have another law for $\overline{u}(x,r)$

$$\boxed{\overline{u}(x,r) = \Delta\overline{u}_m(x)e^{-\frac{r^2}{a(x)^2}}} \tag{7.4.2}$$

With $a(x) = 0.103x$

7.4.3 Species and temperature mixing

Again, the temperature and species mixing are linked to the momentum mixing through the Prandtl number,

$$\frac{\overline{T}(x,r)-T_\infty}{\Delta T_m(x)} = \frac{\overline{C}(x,r)}{C_m(x)} = \left(\frac{\overline{u}(x,r)}{u_m(x)}\right)^{\frac{3}{4}} \tag{7.4.3}$$

By writing the conservation of a species between location $x = 0$ where it has a concentration C_0 and x we get:

$$\int_{r=0}^{R_0} C_0 2\pi r dr = \int_{r=0}^{\infty} \overline{C} 2\pi r dr \tag{7.4.4}$$

$$\Leftrightarrow \quad \frac{C_m(x)}{C_0} = \frac{3R_0^2}{4*(0.103)^2*x^2} \tag{7.4.5}$$

7.4.4 Application to the CFM56 engine used in APEX

The engine used in the experiment has a diameter of approximately $1.4m$ and a bypass ratio of 6. The diameter of the inner core is taken as $\sim 0.4m$

Velocity modeling and validity of the power laws

Let us draw the velocity curves for one power setting

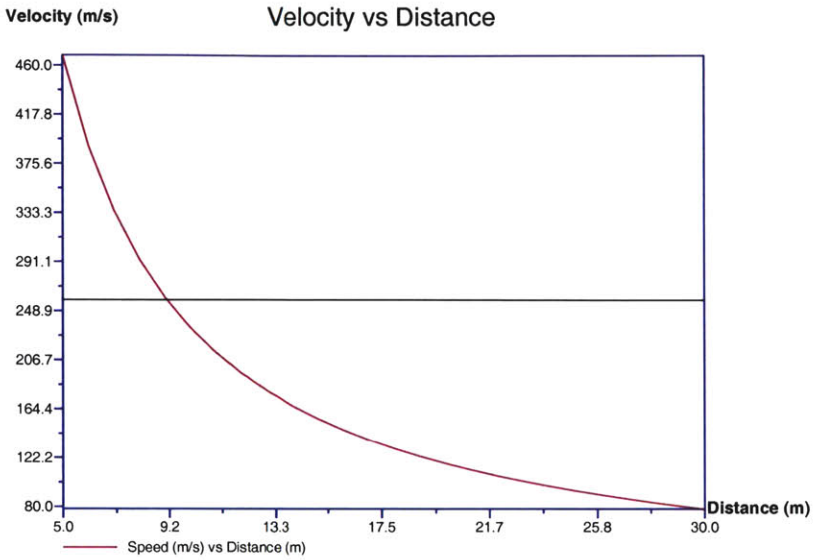

Figure 7.9: Modeled core flow centerline speed if the bypass flow were infinite (occupying all the space around the core flow). The constant line shows the core flow speed at engine exit. The intersection of the two curves shows were the power laws that we used start to be valid. (drawn for 100% Power)

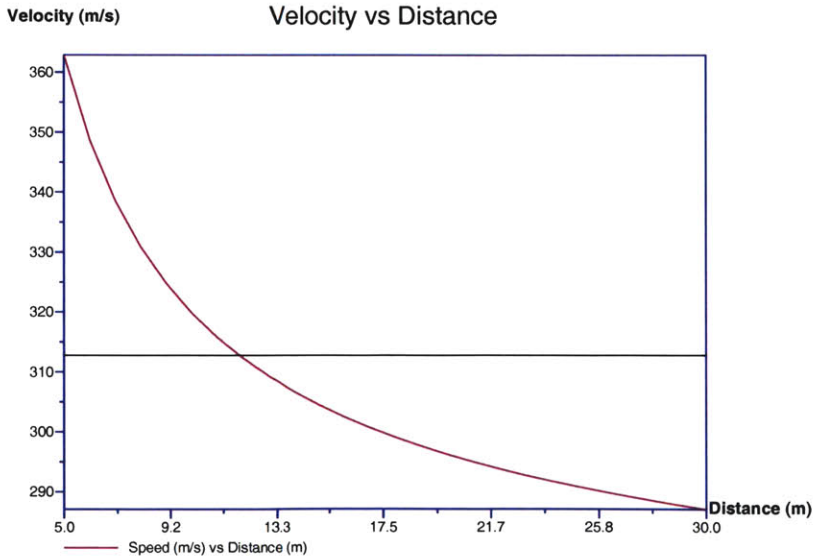

Figure 7.10: Modeled centerline speed if there were no core flow (i.e the core flow had the same speed as the bypass flow). The constant line shows the bypass flow speed at engine exit. The intersection of the two curves shows were the power laws that we used start to be valid. (drawn for 100% Power)

As we see on the above figures, our power laws start to be valid at about $10m$. Before that, we should consider that the centerline flow has not slowed down.

Dilution modeling

Figure 7.11: Dilution ratio $\frac{C_0}{C_m}$ if the bypass flow were infinite (red) and if there were no core flow (blue) (drawn for 100% Power)

Those curves can only help us to determine the dilution after 10 meters as the power laws that we used to obtain them only start to be valid at this point.

We can compare those values with the ones obtained at APEX where the concentration of CO_2 in the exhaust gas enables us to determine the experimental value of the dilution ratio.

Distance \ Power setting	Idle	65%	100%
10m	17.6	14.6	12.0
30m	33.2	23.0	20.4

The 30m values seem suggest that it is the most diluted scenario that is closer to reality. However, these high ratios could be explained by the wind or a misalignment of the probe

with the core flow streamline that can further increase the dilution ratio. Indeed, none of the 10m modeled dilution ratios is close to the 10m measured ratio.

We are facing several modeling issues:

• What should be done for the dilution between $x = 0m$ and $x = 10m$?

There is another power law to help us before 10m:

$$\frac{x_c}{d} = 2.13 Re_d^{0.097} \tag{7.4.6}$$

This law gives the length x_c of the potential core as a function of the diameter of the exhaust and the Reynolds number of the exhaust.

Applied to our case this gives us a potential core length between 2.5m and 3m depending on the power setting, and provides an estimate of when the flow starts to dilute. Between this point and 10m we choose to take a linear interpolation of the dilution. The dilution at 10m will be parameterized between 5 and 20.

• Which one of the dilution curves that we obtained between $x = 10$ and $x = 30m$ is closest to reality?

Even if the experimental data seem to suggest that the most diluted curve is closer to reality, we also choose to parameterize the final dilution ratio at 30 meters as many external effects can explain the high measured value. We parameterize it between 8 and 50.

• What properties of the outside flow are important?

The temperature of the outside flow is an important factor. We choose to parameterize it. We did calculations with outside temperatures of $280K$ $290K$ and $310K$.

At high dilution ratios, the amount of water in the outside flow will account for a significant proportion of the water molecules in the system. We choose the have 80% humidity in the outside flow since data on the humidity during the experiments was not available.

7.5 Thermodynamical modeling of the probe and sampling line

7.5.1 1m samples

In the experiment, the flow sample at 1m was diluted by dry N_2 with a dilution ratio of 25:1 by mass. The N_2 was at an unknown temperature and the probe was cooled with an internal cooling system using tap water at an unknown temperature as the heat sink. Once the flow enters the probe we mix it over 1ms and then allow for up to 10 seconds of reaction time inside the sampling line before the flow reaches the measuring instruments.

7.5.2 10m and 30m samples

The samples taken at 10m and 30m were not further diluted in the experiments. Once the flow entered the probe, its dilution ratio did not vary anymore. The residence time of the flow inside the sampling line was unknown and the temperature was not measured or controlled during this time. We model the sampling line by maintaining a constant temperature and by allowing for up to 10 seconds of reaction time inside the sampling line before the flow reaches the measuring instruments.

7.6 Results

We made many calculations in order to span the wide range of parameters of the modeling: Fuel sulfur content (high sulfur, low sulfur), velocity of the centerline (slowest case, fastest case, or intermediate case), outside air temperature ($280K$, $290K$ or $310K$) dilution ratio at 10m (between 5 and 20), dilution ratio at 30m (between 8 and 50), power setting (Idle, 65%, Take off)

7.6.1 H_2SO_4 production

The emission index of H_2SO_4 per kilogram of fuel is independent of the dilution scenario we choose:

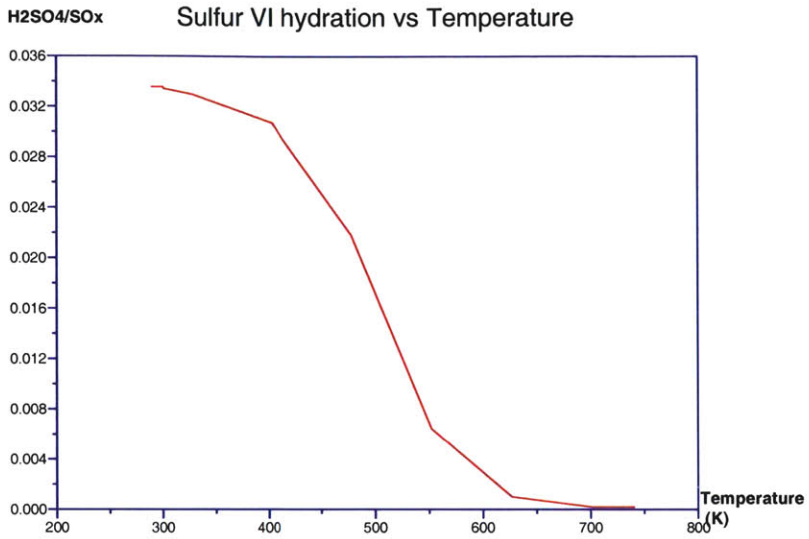

Figure 7.12: percentage of sulfur atoms in H_2SO_4 molecules as a function of the temperature in the plume. On this curve, the flow chronologically goes from the right to the left. This curve is independent of the dilution profile chosen and from the sulfur content.

The SO_3 to H_2SO_4 conversion is a very fast chemistry which has time-scales much smaller than the time-scale associated with the fluid mechanics of the plume (the time the flow spends in the plume before entering the probe is of the order of several tens of milliseconds, whereas the time scale for SO_3 to H_2SO_4 conversion is of the order of less than a millisecond).

We can also see that in the range of final temperatures reached in all our scenarios (289K-350K), the amount of available H_2SO_4 does not vary significantly and is always around 3% of the available sulfur.

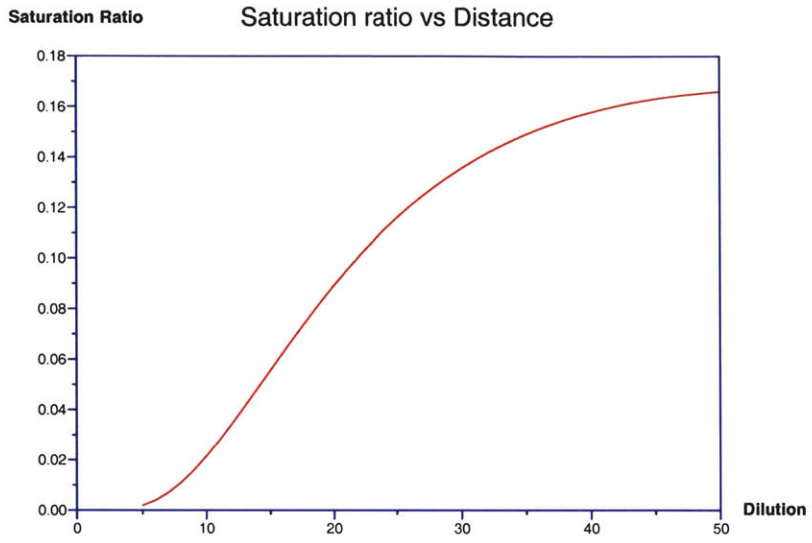

Figure 7.13: Saturation ratio of H_2SO_4 in low sulfur case, as a function of the dilution ratio (core flow temperature at engine exit is $730K$; dilution air temperature is $280K$). The dilution first cools the flow which enables the saturation ratio to increase but the decreasing concentration of H_2SO_4 slows down this effect at higher dilution ratios. This is drawn for the low sulfur content.

7.6.2 Volatile content production

Our results show that the microphysics primarily depends on 2 main parameters:

- The time spent in the sampling line.
- The saturation ratio of H_2SO_4 at the entrance of the probe.

According to the last part, 3% of the sulfur will be available as H_2SO_4. This corresponds to $11mg/kg_{fuel}$ of H_2SO_4 in the low sulfur fuel case and $48mg/kg_{fuel}$ in the high sulfur fuel case. We want to see what proportion of this gets converted to volatile PM.

Creation before entering the probe

The first result of our modeling is that there is little if no creation of volatile content while the flow is in the plume independent of the plume's dilution and speed profile we select. The kinetics of the nucleation process is too slow for the time the flow spends in

the plume ($1ms$ if the sample is taken at 1m, $40ms$ if the sample is taken at $10m$, $120ms$ is the sample is taken at $30m$), and before entering the probe, even in the coldest and slowest case, the volatile emission index predicted by the code was under $10^{-3}mg/kg_{fuel}$.

Creation in the sampling line

Our calculations show that significant gas to particle conversion takes place within the sampling line. They estimate that if the temperature at the entrance of the probe is below a given threshold (330K), the time scales necessary to expect a significant gas to particle conversion are of the order of the second.

For example for a case with a dilution ratio of 48, an outside temperature of 280K and an high sulfur content (molar fraction of water $0.96E-02$, molar fraction of H_2SO_4 $0.604E-07$) . The nucleation characteristics are the following:

number of acid molecules	2
number of water molecules	4
critical radius	0.39nm
nucleation rate	2.55E+05 $particles.cm^{-3}s^{-1}$

and the mole fraction of free H_2SO_4 is given in the following table:

Time (ms)	H_2SO_4 mole fraction (x10^{-7})
150	0.6046
158	0.6046
166	0.6046
175	0.6046
183	0.6046
191	0.6046
200	0.6046
208	0.6046
217	0.6044
225	0.6040
233	0.6028
242	0.5998
250	0.5916
259	0.5701
267	0.5166
275	0.3999
284	0.2153
292	0.6167
301	0.9949
309	0.1308E-02
317	0.1661E-03
326	0.2100E-04
334	0.2653E-05

Table 1. H_2SO_4 mole fraction as a function of time. The time starts at 150ms when the flow enters the sampling system. The flow is then at a temperature of 289K (the coldest temperature reached in our parametarization). After 100ms spent in the sampling system (absolute age 250ms), the mole fraction of H_2SO_4 only dropped by 1%, however, within the next $100ms$ there will be an exponential decrease in the amount of free gaseous H_2SO_4 as condensation on preexisting critical clusters becomes more and more important

The table shows that after some time ($100ms$ in this case) spent within the sampling line during which the consumption of the gaseous H_2SO_4 is slow (1% conversion in 100ms), there is an exponential decrease in the amount of free H_2SO_4. In the coldest case, that will lead to an almost complete consumption of all H_2SO_4 only 180ms after the flow entered the probe. However this time varies with the temperature that the flow reached before entering the probe. If the temperature is above $330K$, the exponential decrease

is never reached even after 10s.

The time the flow has to spend in the sampling line for all the H_2SO_4 to be converted into particulate matter is $180ms$ in the coldest of our cases (temperature of $289K$ at the entrance of the probe) and above $10s$ if the temperature reached at the entrance of the probe is above $330K$. Between those two temperatures, the time necessary to convert the H_2SO_4 is of the order of the second, which is a time that the flow was very likely to have spent in the sampling line during the APEX measurement campaign. We are then able to predict the same amounts of volatile content ($\sim$ tens of milligrams of volatile content per kilogram of fuel burnt) than what was measured during APEX.

7.6.3 Conclusions

The conclusion of this modeling is that we are indeed able to predict the experimental results (creation of volatile content of the order of magnitude of 10mg) but the effect of the sampling system is predominant as the volatile particulate matter is created in the sampling system and not in the plume.

Estimates of the residence times in the plume and in the sampling system show that the residence time of the particles and particulate matter precusors in the sampling line is one or two orders of magnitude higher than in the plume. An aggravating factor is that the time spent in the plume is at an higher temperature.

Ground level measurements have the inconvienence that they are made at ambient temperatures too high for the microphysical evolution time-scales to be faster than the flow time-scale and hence, what is measured at the end of the sampling line is not the same as what entered the probe.

7.7 Recomendations for future work

7.7.1 Temperature sensitivity of the nucleation rate

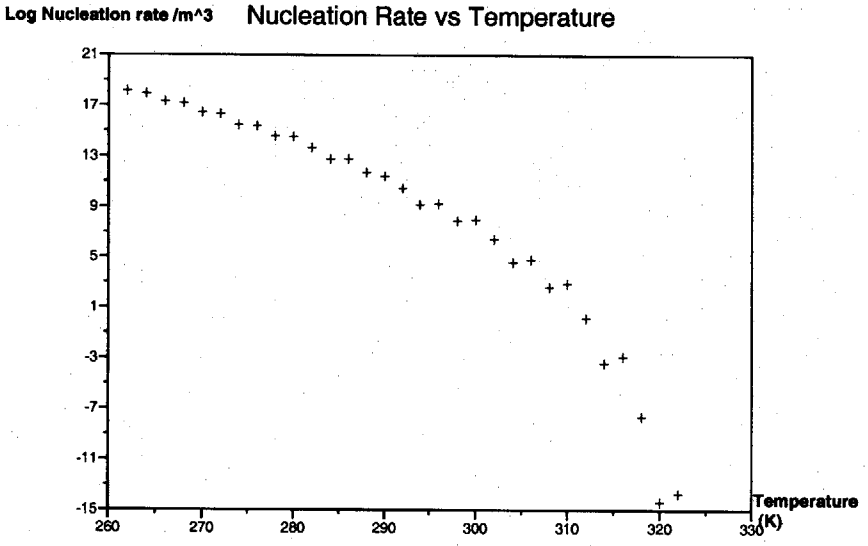

Figure 7.14: Nucleation rate as a function of temperature. The water mole fraction (0.9647E-02) and the sulfuric acid mole fraction (0.6046E-07) are at typical values for a 30m measurement. The nucleation rate is highly sensitive to temperature and can vary greatly in a temperature change of 10 degrees K.

The sensitivity of the nucleation rate with temperature is so large that one has to know the temperature inside the sampling system to properly predict the state of the PM. Contrary to high altitude measurements (where the outside air is at 240-250K), ground level measurements take place at a temperature where the time-scale for nucleation is not in the range of milliseconds (faster than flow time-scales) but rather in the range of seconds (slower than flow time scales).

The temperature being such an important parameter, one should measure it if one wants to have reproduceable results.

7.7.2 Time scales

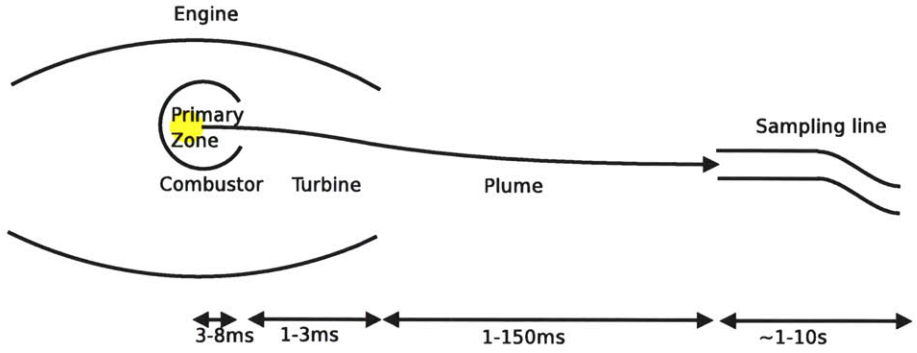

Figure 7.15: Typical flow residence times in different parts of the engine/plume/sampling-system environment

The typical residence times are such that a particle or particulate matter precursor measured at the end of the sampling line will have spent at least 90% of its life within the sampling system. It is from the beginning questionable if such a arrangement can properly transmit particles and particulate matter precursors from one extremity of the sampling system to the other without significant changes in the chemical and microphysical properties of the flow. A reduction of the residence time of the flow to times comparable to or lower than the ones spent in the plume would help prevent dramatic changes in the properties of the flow between the sampling line entrance and sampling line exit.

Bibliography

[1] Anderson, B.E., W.R. Cofer, D.R. Bagwell, J.W. Barrick, C.H. Hudgins, and K.E. Brunke, 1998, "Airborne observations of aircraft aerosol emissions I: Total non-volatile particle emission indices," Geophysical Research Letters, 25(10), pp. 1689-1692.

[2] Anderson, B.E., W.R. Cofer, J.D. Barrick, D.R. Bagwell, and C.H. Hudgins, 1998, "Airborne observations of aircraft aerosol emissions II: Factors controlling volatile particle production," Geophysical Research Letters, 25(10), pp. 1693-1696.

[3] Anderson, B.E., W.R. Cofer, J. Crawford, G.L. Gregory, S.A. Vay, K.E. Brunke, Y. Kondo, M. Koike, H. Schlager, S.L. Baughcum, E. Jensen, Y.J. Zhao, and K. Kita, 1999, "An assessment of aircraft as a source of particles to the upper troposphere," Geophysical Research Letters, 26(20), pp. 3069-3072.

[4] Arnold, F., A. Kiendler, V. Wiedemer, S. Aberle, T. Stilp, and R. Busen, 2000, "Chemiion concentration measurements in jet engine exhaust at the ground: Implications for ion chemistry and aerosol formation in the wake of a jet aircraft," Geophysical Research Letters, 27(12), pp. 1723-1726.

[5] Ball, R.T. and J.B. Howard, 1971, Electric charge of carbon particles in flames, Thirteenth International Symposium on Combustion, Combustion Institute, Pittsburg, Pennsylvania, pp. 353-362.

[6] Brock, C.A., F. Schroder, B. Karcher, A. Petzold, R. Busen, and M. Fiebig, 2000, "Ultrafine particle size distributions measured in aircraft exhaust plumes," Journal of Geophysical Research-Atmospheres, 105(D21), pp. 26555-26567.

[7] Brown, R.C., M.R. Anderson, R.C. MiakeLye, C.E. Kolb, A.A. Sorokin, and Y.Y. Buriko, 1996, "Aircraft exhaust sulfur emissions," Geophysical Research Letters, 23(24), pp. 3603-3606.

[8] Fialkov, A.B., 1997, "Investigations on ions in flames," Progress in Energy and Combustion Science, 23, pp. 399-528.

[9] Fuchs, N., 1964, The mechanics of aerosols, Dover, Mineola, New York.

[10] Goebel, S.G., N. Abuaf, J.A. Lovett, and C.-P. Lee, 1993, Measurement of combustor velocity and turbulence profiles, ASME 93-GT-228, Twelfth International Symposium on Combustion, Pittsburg, Pennsylvania

[11] Hagen, D., P. Whitefield, J. Paladino, M. Trueblood, and H. Lilenfeld, 1998, "Particulate sizing and emission indices for a jet engine exhaust sampled at cruise," Geophysical Research Letters, 25(10), pp. 1681-1684.

[12] Haverkamp, H., S. Wilhelm, A. Sorokin, and F. Arnold, 2004, "Positive and negative ion measurements in jet aircraft engine exhaust: concentrations, sizes and implications for aerosol formation," Atmospheric Environment, 38(18), pp. 2879-2884.

[13] Hoppel, W.A. and G.M. Frick, 1986, "Ion-aerosol attachment coefficient and the steady-sate charge distribution on aerosol in bipolar ion environment," Aerosol Science and Technology, 5, pp. 1-21.

[14] Howard, J.B., 1969, On the Mechanism of Carbon Formation in Flames, Twelfth international symposium on combustion, Combustion Institute, Pittsburg, PA, pp. 877-887.

[15] Howard, J.B., B.C. Wersborg, and G.C. Williams, 1973, Coagulation of Carbon Particles in Premixed Flame, Faraday Symposium of the Chemical Society, Chemical Society, pp. 109-119.

[16] ICAO, 1995, "Engine exhaust emissions data bank, 1st edition with amendments," ICAO-9646-AN/943, International Civil Aviation Organization, Montreal, Canada.

[17] Intergovernmental Panel on Climate Change, IPCC, 1999, "Aviation and the global atmosphere: A special report of the Intergovernmental Panel on Climate Change," J.E. Penner, D.H. Lister, D.J. Griggs, D.J. Dokken, and M. McFarland, eds., Cambridge University Press, Cambridge, UK.

[18] Jaecker-Voirol A.,P. Mirabel, 1987, "Hydrates in supersaturated binary sulfuric acid-water vapor: A reexamination", Journal of Chemical Physics, 87(8), pp.4849-4852.

[19] Karcher, B., 1998, "Physicochemistry of aircraft-generated liquid aerosols, soot, and ice particles - 1, Model description," Journal of Geophysical Research-Atmospheres, 103(D14), pp. 17111-17128.

[20] Konopka, P., U. Schumann, H. Schlager, D. Hagen, P. Whitefield, and J. Ovarlez, 1997, "Particulate emissions of commercial jet aircraft under cruise conditions, Report 91," Institut für Physik der Atmosphäre, eds., DLR

[21] Kulmala M., A. Laaksonen, 1990, "Binary nucleation of water-sulfuric acid system: Comparison of classical theories with different H_2SO_4 saturation vapor pressures, Journal of Chemical Physics, 93(1), pp.696-701

[22] Lukachko, S.P., I.A. Waitz, R.C. Miake-Lye, and R.C. Brown, 2005, "Engine design and operational impacts on aircraft particulate matter precursor emissions," GT2005-69112, ASME Turbo Expo 2005, American Society of Mechanical Engineers, Reno-Tahoe, Nevada.

[23] Lukachko, S.P., I.A. Waitz, R.C. Miake-Lye, R.C. Brown, and M.R. Anderson, 1998, "Production of sulfate aerosol precursors in the turbine and exhaust nozzle of an aircraft engine," Journal of Geophysical Research-Atmospheres, 103(D13), pp. 16159-16174.

[24] Marquart, S. and B. Mayer, 2002, "Towards a reliable GCM estimation of contrail radiative forcing," Geophysical Research Letters, 29(8).

[25] Marquart, S., M. Ponater, F. Mager, and R. Sausen, 2003, "Future development of contrail cover, optical depth, and radiative forcing: Impacts of increasing air traffic and climate change," Journal of Climate, 16(17), pp. 2890-2904.

[26] Maxwell, J.C., 1954, A treatise on electricity and magnetism, Dover, New York, New York.

[27] Meyer, R., H. Mannstein, R. Meerkotter, U. Schumann, and P. Wendling, 2002, "Regional radiative forcing by line-shaped contrails derived from satellite data," Journal of Geophysical Research-Atmospheres, 107(D10).

[28] Miake-Lye, R.C., B.E. Anderson, W.R. Cofer, H.A. Wallio, G.D. Nowicki, J.O. Ballenthin, D.E. Hunton, W.B. Knighton, T.M. Miller, J.V. Seeley, and A.A. Viggiano, 1998, "SOx oxidation and volatile aerosol in aircraft exhaust plumes depend on fuel sulfur content," Geophysical Research Letters, 25(10), pp. 1677-1680.

[29] Miake-Lye, R.C., M. Martinez-Sanchez, R.C. Brown, and C.E. Kolb, 1993, "Plume and Wake Dynamics, Mixing, and Chemistry Behind a High-Speed Civil Transport Aircraft," Journal of Aircraft, 30(4), pp. 467-479.

[30] Mick, H.J., A. Hospital, and P. Roth, 1991, "Computer simulation of soot particle coagulation in low pressure flames," Journal of Aerosol Science, 22(7), pp. 831-841.

[31] Minnis, P., J.K. Ayers, R. Palikonda, and D. Phan, 2004, "Contrails, cirrus trends, and climate," Journal of Climate, 17(8), pp. 1671-1685.

[32] Nickels T.B., A.E. Perry, 1996, "An experimmental and theoritical study of the turbulent coflowing jet", Journal of fluid mechanics, 309, pp.157-182

[33] Noppel M., 1998, "Binary nucleation of water-sulfuric system: A reexamination of the classical hydrates interaction model, Journal of Chemical Physics, 109(20), pp.9052-9056

[34] Noppel M., H. Vehkamaki, and M. Kulmala, 2001, "An improved model for hydrate formation in sulfuric acid-water nucleation", Journal of Chemical Physics, 116(1), pp.218-228

[35] Petzold, A., M. Fiebig, L. Fritzsche, C. Stein, U. Schumann, C.W. Wilson, C.D. Hurley, F. Arnold, E. Katragkou, U. Baltensperger, M. Gysel, S. Nyeki, R. Hitzenberger, H. Giebl, K.J. Hughes, R. Kurtenbach, P. Weisen, P. Madden, H. Puxbaum, S. Vrchoticky, and C. Wahl, 2003, Particle emissions from aircraft engines, An overview of the European project PartEmis, European Conference on Aviation, Atmosphere, and Climate (AAC), Proceedings of an International Conference, European Commission, Friedrichshafen, Germany, pp. 41-51.

[36] Pruppacher, H.R. and J.D. Klett, 1978, Microphysics of clouds and precipitation, D. Reidel Publishing Company, Dordrecht, Holland.

[37] Pueschel, R.F., S. Verma, G.V. Ferry, S.D. Howard, S. Vay, S.A. Kinne, J. Goodman, and A.W. Strawa, 1998,"Sulfuric acid and soot particle formation in aircraft exhaust," Geophysical Research Letters, 25(10), pp. 1685-1688.

[38] Rodi W., 1975, Studies in convection, Academic Press, London

[39] Saffman, P.G. and J.S. Turner, 1955, "On the collision of drops in turbulent clouds," Journal of Fluid Mechanics, 1.

[40] Schroder, F., B. Karcher, C. Duroure, J. Strom, A. Petzold, J.F. Gayet, B. Strauss, P. Wendling, and S. Borrmann, 2000, "On the transition of contrails into cirrus clouds," Journal of the Atmospheric Sciences, 57(4), pp. 464-480.

[41] Schumann, U., F. Arnold, R. Busen, J. Curtius, B. Karcher, A. Kiendler, A. Petzold, H. Schlager, F. Schroder, and K.H. Wohlfrom, 2002, "Influence of fuel sulfur on the composition of aircraft exhaust plumes: The experiments SULFUR 1-7," Journal of Geophysical Research-Atmospheres, 107(D15).

[42] Schumann, U., H. Schlager, F. Arnold, J. Ovarlez, H. Kelder, O. Hov, G. Hayman, I.S.A. Isaksen, J. Staehelin, and P.D. Whitefield, 2000, "Pollution from aircraft emissions in the North Atlantic flight corridor: Overview on the POLINAT projects," Journal of Geophysical Research-Atmospheres, 105(D3), pp. 3605-3631.

[43] Seinfeld, J.H. and S.N. Pandis, 1997, Atmospheric chemistry and physics, Wiley-Interscience.

[44] Sorokin, A. and F. Arnold, 2004, "Electrically charged small soot particles in the exhaust of an aircraft gas-turbine engine combustor: comparison of model and experiment," Atmospheric Environment, 38(17), pp. 2611-2618.

[45] Spicer, C.W., M.W. Holdren, R.M. Riggin, and T.F. Lyon, 1994, "Chemical-Composition and Photochemical Reactivity of Exhaust from Aircraft Turbine-Engines," Annales Geophysicae-Atmospheres Hydrospheres and Space Sciences, 12(10-11), pp. 944-955.

[46] Starik, A.M., A.M. Savel'ev, N.S. Titova, and U. Schumann, 2002, "Modeling of sulfur gases and chemiions in aircraft engines," Aerospace Science and Technology, 6(1), pp. 63-81.

[47] Stauffer D., 1976, "Kinetic theory of two-component ("Heteromolecular") nucleation and condensation", Journal of Aerosol Science, 7, pp. 319-333

[48] Taleb D., J. Ponche, P. Mirabel, 1996, "Vapor pressures in the ternary system water-nitric acid-sulfuric acid at low temperature: A reexamination", Journal of geophysical research, 101, pp.25967-25977

[49] Travis, D.J., A.M. Carleton, and R.G. Lauritsen, 2002, "Climatology: Contrails reduce daily temperature range - A brief interval when the skies were clear of jets unmasked an effect on climate," Nature, 418(6898), pp. 601-601.

[50] Tremmel, H.G. and U. Schumann, 1999, "Model simulations of fuel sulfur conversion efficiencies in an aircraft engine: Dependence on reaction rate constants and initial species mixing ratios," Aerospace Science and Technology, 3(7), pp. 417-430.

[51] U.S. Federal Aviation Administration, FAA, 2003, "Select resource materials and annotated bibliography on the topic of hazardous air pollutants (HAPs) associated with aircraft, airports, and aviation," Federal Aviation Administration, Office of Environment and Energy, Prepared by URS Corporation, Washington, D.C.

[52] U.S. National Institute of Standards and Technology, NIST, 2003, NIST Chemistry WebBook: NIST Standard Reference Database Number 69, W.G. Mallard, eds., Data available online at http://webbook.nist.gov/chemistry, U.S. Department of Commerce.

[53] Vehkamaki H., M. Kulmala, K.E.J. Lehtinen, and M. Noppel, 2003, "Modelling binary homogeneous nucleation of water-sulfuric acid vapours: Parametetisation for high temperature emissions", Environmental Science and Technology 37(15), pp.3392-3398

[54] Vehkamaki H, M. Kulmala, I. Napari, K.E.J. Lehtinen, C. Timmreck, M. Noppel, A. Laaksonen, 2002, "An improved parameterization for sulfuric acid-water nucleation rates for tropospheric and stratospheric conditions", Journal of Geophysical Research, 107(D22), pp.4622-4632

[55] Viisanen Y., M. Kulmala, and A. Laaksonen,1997, "Experiments on gas-liquid nucleation of sulfuric acid and water", Journal of Chemical Physics, 107(3), pp.920-926

[56] Whitefield, P., D.E. Hagen, K. Brundish, A.R. Clague, C.W. Wilson, R.C. Miake-Lye, R.C. Brown, J. Wormhoudt, S.P. Lukachko, A.T. Chobot, C.K. Yam, and I.A. Waitz, 2002, "NASA/QinetiQ Collaborative Program, Final Report," NASA CR-2002-211900, NASA Glenn Research Center, U.S. National Aeronautics and Space Administration, Cleveland, Ohio.

[57] Wilson, C.W., A.R. Clague, M. Pourkashanian, and L. Ma, 2004, "Chemical kinetic modeling of the evolution of gaseous aerosol precursors within a gas turbine engine," GT2004-53704, ASME Turbo Expo 2004, American Society of Mechanical Engineers, Vienna, Austria.

[58] Yu, F.Q., R.P. Turco, and B. Karcher, 1999, "The possible role of organics in the formation and evolution of ultrafine aircraft particles," Journal of Geophysical Research-Atmospheres, 104(D4), pp. 4079-4087.